Evaluating effects of the terrain on modelled winds in multiple atmospheric model datasets

Maksims Pogumirskis[1, 2], Tija Sīle[1], Lasse Svenningsen[2], and Andrea N. Hahmann[3]

[1]Institute of Numerical Modelling, Faculty of Science and Technology, University of Latvia, Riga, Latvia
[2]EMD International A/S, Aalborg, Denmark
[3]Wind Energy Department, Technical University of Denmark, Roskilde, Denmark

Correspondence: Maksims Pogumirskis (maksims.pogumirskis@lu.lv)

Abstract. Numerical atmospheric models are widely used as a meteorological data source when planning the locations of new wind farms. However, before relying on model output for decision-making, it must be verified against observations. Due to commercial restrictions on the availability of observation data, previous studies on atmospheric model validation for wind energy applications are often limited to a single model or a small geographical region. This work performs a large-scale bias assessment of modelled winds at wind turbine heights from seven model datasets against data from more than 500 observation campaigns across Europe. Principal component analysis is used to identify spatial, diurnal, and seasonal patterns of wind speed and direction biases. The results of the analysis show that all seven models exhibit similar spatial and temporal patterns of wind speed bias. Models generally show a more positive wind-speed bias in the Central European Plain and a more negative bias in mountainous regions, namely Southern Europe and the Scandinavian Mountains. Moreover, the temporal patterns of biases also differ between these regions, and wind direction bias shows the same temporal and spatial patterns as the wind speed bias. We show that these wind speed and direction biases can be explained by differences in terrain height between the models and the real world. The magnitude of the wind speed bias ranges from 0.1 to 0.9 ms^{-1} per 100 m of elevation difference, depending on the season and time of day. Two WRF model simulations with different terrain source data are performed, and the modelled winds are compared to provide more robust support for the hypothesis. The results of this work suggest that improving terrain representation in mesoscale models can help improve their performance.

1 Introduction

Global warming, which is primarily driven by anthropogenic greenhouse gases, is a major threat to both humans and ecosystems. In 2016, 196 countries signed the Paris agreement with goals of limiting global warming to 2 °C, preferably 1.5 °C, compared to pre-industrial levels (United Nations Climate Change (UNFCCC)). In pursuit of implementing the agreement, the European Union has set the goal of reaching 45 % share of renewable energy by 2030. To meet the goal, it is estimated that wind turbines with a total cumulative capacity of at least 37 GW have to be installed each year (European Commission, 2023).

Wind farms require high upfront investments, which are offset by significantly lower operating costs than fossil fuel plants. Therefore, in the planning stages it is important to ensure that they will provide stable and reliable power output throughout their lifetime. This is needed to ensure financial profit, keep electricity prices stable and keep the electricity supply reliable and

predictable (Backwell et al., 2025; Williams et al., 2025). When planning the locations of new wind farms, it is necessary to acquire precise information about the wind climate at their potential locations. Wind power density is proportional to the cube of wind speed. Therefore, a small error in the wind speed estimates of 5 % can cause an error of up to 15 % when estimating wind power production.

Direct measurements are commonly used for wind resource assessment. While the World Meteorological Organization (WMO) observation station network is broad and uniformly covers most of the land, it provides only surface wind observations at 10 m height, which are less useful for estimating the wind at turbine heights. The wind measurement network for wind turbine heights is much scarcer than the synoptic network (Ramon et al., 2020). According to MEASNET (2022), for the assessment of site-specific conditions, wind speed measurements are required at a minimum height of 2/3 of the height of the turbine hub. Preferably, measurement heights should span the entire rotor area. The heights of modern wind turbines exceed 200 m, making the use of tall masts impractical for wind resource assessment at higher levels (Cheynet et al., 2025). Although lidars allow one to acquire wind data at higher levels more easily, they are unreliable in case of fog or strong rain (Knoop et al., 2021). Moreover, to acquire a meaningful amount of data, the measurement campaign has to be performed for at least a year, which requires regular equipment maintenance. Wind measurements are highly sensitive to the terrain and other obstacles in close proximity. According to MEASNET (2022), for homogeneous surface roughness conditions, mast observations are representative for a radius of 2 km in complex terrain and 10 km in simple terrain. Therefore, a separate measurement campaign has to be conducted at each potential wind farm location.

Numerical modelling is an alternative way to acquire information about the wind conditions at a site, and it has several advantages over direct measurements. It allows to produce spatially and temporally continuous wind data. Moreover, running numerical models is much faster and cheaper than performing measurements. However, results of numerical models should not be relied on without verifying that they match observations, and their limitations are well understood.

Previous studies that have compared atmospheric models against observations for wind energy applications are usually limited to a single model, e.g. CERRA (Jourdier et al., 2023; Rouholahnejad et al., 2024), NEWA (Dörenkämper et al., 2020; Meyer and Gottschall, 2022), NORA3 (Solbrekke et al., 2021), or multiple models in a limited geographical region, e.g., France (Jourdier, 2020), Sweden (Kuru, 2023; Zhi, 2023), North Sea (Cheynet et al., 2022; Spangehl et al., 2023; Kalverla et al., 2020). It has been identified that atmosphere models have systematic issues in representing the observed wind climate.

Model ability to resolve flows affected by terrain is largely dependent on their spatial resolution. Synoptic scale models usually have horizontal grid spacings of several tens of kilometres, cover the entire globe and are designed to capture large-scale synoptic features such as anticyclones, cyclones and fronts. Typical effective resolution of synoptic scale models is approximately 3-4 times their grid resolution (Klaver et al., 2020). Smaller scale processes than the effective resolution might not be properly simulated. Studies have shown that due to their coarse resolution, synoptic scale models generally perform worse in complex terrain (Das and Baidya Roy, 2024) or near complex coastlines (Gualtieri, 2021).

To improve modelled winds in regions with complex land properties, mesoscale modelled datasets are created by dynamically downscaling synoptic scale model output. Mesoscale models usually have horizontal grid spacings of a few kilometres, cover only a limited area, and can capture winds on finer scales. The effective resolution of the WRF mesoscale model is

approximately 7 times its grid resolution (Skamarock, 2004). Studies have shown that mesoscale models outperform synoptic scale models, especially when modelling extreme winds (Solbrekke et al., 2021) or winds in complex terrain (Dörenkämper et al., 2020).

Both synoptic scale and mesoscale models commonly use terrain following coordinates, which can introduce numerical artefacts in steep terrain (Shaw and Weller, 2016) and therefore might require applying additional smoothing to the model terrain (Bouëdec et al., 2025). Smoothing of the terrain can worsen the representation of fine features of the terrain, such as narrow valleys (Schmidli et al., 2018). To better resolve the effects of complex terrain features, microscale modelling can be performed. Typical horizontal grid spacing of microscale models is on the order of tens of metres. In addition, in microscale models, fine terrain features can be resolved by performing local mesh refinement using unstructured meshes (Yamaguchi et al., 2024) or immersed boundary methods (jaf, 2011). The major downside of microscale models is that they are computationally expensive and cannot be directly used to produce long-term wind time series.

In this work, we perform a large-scale bias assessment of seven atmospheric model datasets for wind energy applications. Winds at heights relevant for wind energy from three global reanalyses and four mesoscale datasets are compared with observations from 508 observation campaigns covering the entire Europe. The aim of the analysis is to identify key systematic differences between modelled and observed winds and physically explain their potential causes. For this purpose, model wind speed biases are analysed in context with wind direction biases. Principal component analysis is used to identify the principal diurnal, seasonal, and spatial patterns of wind speed and direction biases. We explain these wind biases by the terrain elevation differences between models and the real-world.

Several studies have assessed model performance at individual observation sites in complex terrain. Performance at a particular observation site largely depends on the model dataset (Cheynet et al., 2025). Fernández-González et al. (2018) has observed that the overall model performance in complex terrain increases with increasing model resolution. On the other hand, Solbakken et al. (2021) has observed that increasing model resolution from 3 km to 1 km does not improve model performance metrics. However, it allows the model to resolve certain features of the wind climate. It has been shown that model performance largely depends on geographical location, atmospheric stability and wind conditions (Weigel et al., 2008). Therefore, studies that use data from only a few observation sites cannot be reliably used to draw general conclusions about model performance in complex terrain, even if they cover various terrain types (Jourdier, 2020).

Large scale comparisons are needed to draw general conclusions regarding model performance in different terrain types. Previous studies that performed large scale comparisons between modelled and observed wind speeds have identified that models generally show stronger biases in complex terrain. However, most of these large-scale studies focus on 10 m winds and not on the heights relevant to wind energy. Laurila et al. (2021) has observed that ERA5 underestimates the wind speed in complex terrain. Le Toumelin et al. (2024) has observed that the same is true for the AROME model. Dörenkämper et al. (2020) has shown that both ERA5 and NEWA show more negative biases in locations with a higher terrain ruggedness index (RIX). The magnitude of bias in NEWA is smaller than the one in ERA5. Hu et al. (2023) has shown that ERA5 generally shows stronger biases in complex terrain. Das and Baidya Roy (2024) has compared models with wind speed observations in

India. It was shown that multiple global reanalyses significantly overestimated winds in complex terrain, while showing lower bias in simpler terrain.

Studies have identified that wind speed biases in models differ based on the relative topographic position, i.e. valleys, plains, ridges, etc.. Winstral et al. (2016) has observed that COSMO models show a positive wind speed bias in valleys and a negative bias on upper slopes and ridges. Jiménez and Dudhia (2012) has observed that WRF model overestimates wind speeds inside the valleys and in plains, while underestimating them on hilltops. On the other hand, Gómez-Navarro et al. (2015) has shown that WRF models generally overestimate wind speeds regardless of the relative topographic position.

Several possible causes of wind speed biases in synoptic scale and mesoscale models in complex terrain have been documented in the literature. Das and Baidya Roy (2024) attributes wind speed biases in complex terrain to model inability to resolve small scale terrain features. Cheynet et al. (2025) has explained model biases by their inability to resolve processes characteristic to complex terrain, such as recirculation and detached flows. Sandu et al. (2017) explains model biases by their errors in estimating orographic drag. Gómez-Navarro et al. (2015) attributes model biases in complex terrain to errors in estimating the effects of unresolved topography. The results of Jiménez and Dudhia (2012) suggest that wind speed biases in complex terrain are caused by errors in estimating the orographic speed-up. Moreover, a representativeness bias is present in models, since the nearest model grid-cell is not always the most representative of the actual observation site.

Previous small scale studies (Schmidli et al., 2018; Carvalho et al., 2012; Saadatabadi et al., 2024) have suggested that models perform better if the absolute difference between the model and the real-world terrain elevation is lower. In this work, we attempt to explain those model biases that are related to relative topographic position (hilltops, plains, valleys) of the observation site by the elevation difference between the model and the real-world. Namely, due to terrain aggregation and smoothing in atmospheric models, terrain elevation in models is generally above the real-world elevation for observation sites inside valleys, and terrain elevation in models is generally below the real-world elevation for observation sites on hilltops. It is further shown that the elevation difference has an effect not only on the average wind speed bias, but also on the wind direction bias and their diurnal and seasonal cycles. Two WRF model simulations with different terrain source data are performed, and the modelled winds are compared to show that model wind biases can potentially be improved by adjusting their terrain elevation.

Further in the work it is discussed which physical processes are potentially affected by the difference in the terrain elevation between models and the real-world. However, regardless of the exact physical cause of the bias, the correlation between model bias and the elevation difference between the model and the real-world suggests that improving terrain representation in atmospheric models has the potential to improve their performance in modelling winds.

The work is structured as follows: subsection 2.1 describes model and observation datasets used, subsubsection 2.2.1 describes methods used when comparing models with observations, subsubsection 2.2.2 describes principal component analysis (PCA) method used for bias assessment, subsubsection 2.2.3 describes how we use terrain data in explaining model biases, subsubsection 2.2.4 describes WRF numerical model setup that we used and numerical experiments that we performed, subsection 3.1 describes the results of the comparison between models and observations, subsection 3.2 describes the results of the comparison between two models, discussion of the results is presented in section 4, and conclusions are presented in section 5.

2 Data and methods

2.1 Data

2.1.1 Model datasets

In this work, the winds from seven different model datasets were compared against the observations. This includes three global reanalyses: ERA5, MERRA2 and JRA-3Q and four mesoscale model datasets derived from the ERA5 reanalysis by performing dynamical downscaling: NORA3, CERRA, NEWA, and EMD-EUR+. General information about model datasets is compiled in Table 1.

The ERA5 (Hersbach et al., 2020) is a global reanalysis developed by the European Centre for Medium-range Weather Forecasts (ECMWF). ERA5 is based on the Integrated Forecasting System (IFS) modelling system. It provides hourly data of the estimated state of the atmosphere with a resolution of 0.25°or ≈28 km in latitudinal direction. Such a resolution is one of the finest for global reanalyses. Wind speed data on constant height levels in ERA5 are limited to only 10 m and 100 m, which is fewer levels than in the case with mesoscale models. Additionally, near surface wind data from ERA5 are available on pressure levels or native model levels. Due to temporal variation of the atmospheric pressure, the geopotential height of a constant pressure level can vary by more than 100 m and sometimes go below ground level, which makes the use of wind data on constant pressure levels inconsistent for our purposes. Access to the ERA5 data on native model levels is provided separately from the re-gridded data on height and pressure levels and is much slower. Therefore, for simplicity and consistency, in this work only 10 m and 100 m winds from the ERA5 were used.

There is a known systematic issue with winds at lower model levels in the ERA5. Jourdier (2020) has shown that 10 m, 100 m and lower model level winds in ERA5 experience a sudden artificial drop in value at the start of the assimilation window at 9:00 UTC. Wind speeds slowly recover by the end of the assimilation window at 21:00 UTC. Downscaled mesoscale products can potentially inherit the issue, as they use initial and boundary conditions from ERA5. While this issue is not the main focus of the study, it was briefly examined whether or not it is inherited in downscaled mesoscale models.

The NEWA (Hahmann et al., 2020) is a mesoscale atmospheric dataset based on the open-source Weather Research and Forecasting (WRF) modelling system. It has been developed as an ERANET+ project. The model is run on 27–9–3 km nested domains, where the outer low-resolution domain provides boundary conditions for inner domains. The outer 27 km domain covers a region beyond Europe. A total of ten different overlapping smaller 9–3 km nested domains are used to cover the region of interest. The final dataset with 3 km grid spacing is acquired by spatially stitching together results from all ten 3 km domains and extends over the European Union, the United Kingdom, Norway, Switzerland, Balkans, Turkey, and nearby offshore areas. NEWA provides output every 30 minutes. However, to match other model datasets, only data at full hours were used.

The WRF model used in NEWA is reinitialised every 7 days and run for 8 days. The first 24 hours are used as a spin-up time, and therefore discarded. Meanwhile, the remaining 7 days contribute to the dataset. Spectral nudging to ERA5 reanalysis is performed in the outer domain only above the planetary boundary layer. The NEWA simulations use boundary conditions and nudging data derived from 6-hourly ERA5 data.

The EMD-WRF EUROPE+ (or EMD-EUR+ for short) (Svenningsen et al., 2020) mesoscale dataset is developed by EMD International A/S. It is based on the WRF modelling system and run on a single large 3 km domain without nesting that covers the entire Europe. The model is reinitialised every 7 days and uses a spin-up time of 24 hours. Spectral nudging to the ERA5 reanalysis is performed above the planetary boundary layer. The EMD-EUR+ simulations use boundary conditions and nudging data derived from hourly ERA5 data.

The CERRA (Ridal et al., 2024) is a mesoscale reanalysis developed by ECMWF. It is based on the HARMONIE-ALADIN modelling system configuration. It has a coarser grid spacing (5.5 km) than the other mesoscale models used. The CERRA dataset provides atmospheric analysis using 3D-VAR data assimilation every 3 hours. Additionally, after each data assimilation, a 6-hour forecast with hourly output is provided. The forecast is extended to 30 hours twice a day: at 0:00 and 12:00 UTC. Documentation of the dataset leaves the choice open for the user on which data to use, when constructing hourly series (Jourdier et al., 2023). In this work, hourly series series were constructed using only forecasts with 1, 2, and 3 hour lead-times.

The NORA3 (Haakenstad et al., 2021) is a mesoscale model developed by the Norwegian Meteorological Institute. It is based on the HARMONIE-AROME modelling system configuration and has a spatial grid spacing of 3 km. While other mesoscale datasets used in this work cover the entire Europe, NORA3 covers only the northern part of it. NORA3 is run as a hindcast, which is initialised every 6 hours using data from ERA5 reanalysis. The hindcast is run for 9 hours, using the first 3 hours as a spin-up time. NORA3 assimilates only temperature and air humidity observations. The upper-air temperature, humidity, and wind components are interpolated from the host reanalysis ERA5.

The MERRA2 (Gelaro et al., 2017) is a global reanalysis developed by the National Aeronautics and Space Administration (NASA). MERRA2 is based on Goddard Earth Observing System (GEOS) modelling system. It provides hourly atmospheric data with $0.5^\circ \times 0.625^\circ$ resolution. For similar reasons as with ERA5, we used winds from MERRA2 only on constant height levels, which are 10 m and 50 m AGL.

The JRA-3Q (Kosaka et al., 2024) is a global reanalysis developed by the Japanese Meteorological Agency (JMA) and is based on the JMA global Numerical Weather Prediction (NWP) system. The spatial resolution of the JRA-3Q is 0.375°. JRA-3Q provides the analysis of the atmosphere every 6 hours. Additionally, forecast data with 3 and 6 hour lead-times are provided. For consistency purposes, in this work, 3-hourly time series were constructed using only forecast data. The only height level at which JRA-3Q outputs winds is 10 m. However, JRA-3Q reanalysis provides data on 8 native model levels in the lowest approximately 300 m of the atmosphere. Therefore, wind data together with geopotential data on native model levels were used. As the model is run on hybrid vertical levels, exact heights AGL of these levels differ between model time-steps and geographical locations.

Although JRA-3Q was released in 2018, studies that have assessed its performance for wind energy applications are limited to China (Mi and Liu, 2024). This is likely due to the fact that it is only licenced for non-commercial use. However, its predecessor JRA55 has been widely validated for wind energy applications, e.g. Miao et al. (2020); Das and Baidya Roy (2024). While JRA55 has generally shown poorer performance than ERA5 in modelling winds at turbine heights (Ramon et al., 2019), JRA55 uses significantly different approaches when modelling winds than other global reanalyses. Firstly, based on the results of Carvalho (2019); Belmonte Rivas and Stoffelen (2019), JRA55 is the only global reanalysis that did not

Table 1. Summary of model datasets and their characteristics.

Model	Horizontal grid spacing	Height levels used, m	Temporal resolution, h	Vertical levels	Region	Modelling system
ERA5	0.25°	10, 100	1	137	Global	IFS
MERRA2	0.5°× 0.625°	10, 50	1	72	Global	GEOS
JRA-3Q	0.375°	8 native model levels	3	100	Global	JMA global NWS
NORA3	3 km	50, 100, 250	1	65	Northern Europe	HARMONIE
NEWA	3 km	50, 75, 100, 150, 200	0.5 (1 used)	61	Europe	WRF
CERRA	5.5 km	50, 75, 100, 150, 200	1	106	Europe	HARMONIE
EMD-EUR+	3 km	50, 75, 100, 150, 200	1	50	Europe	WRF

show systematic clockwise wind direction bias over the oceans in the Northern Hemisphere, which is a long-known issue in atmospheric models (Hollingsworth, 1994). Secondly, as reported by Torralba et al. (2017), JRA55 is the only global reanalysis that assimilates surface wind speed observations over the land, which allows JRA55 to show good performance in modelling inter-annual wind speed variation and trends on decadal timescales.

2.1.2 Observation dataset

In this work, to evaluate the model biases, we compare the model output against the EMD's internal database of wind mast data. The database contains time-series of wind observations from wind masts and remote sensing devices since the 1980's at different heights up to 300 m above ground level (AGL). The database contains data from over 1000 observation locations around the globe.

This work focuses on Europe. When discussing the results of the work, regions of Europe are referred to as shown in Figure 1. Due to data confidentiality, exact locations of observation locations cannot be disclosed. The region of interest and the approximate number of observation locations per country are shown in Figure 2. It should be noted that offshore measurement campaigns were also included in the work, which are counted towards the country in which exclusive economic zone it is located. In further figures, results are aggregated into hexagonal bins to present spatial patterns of biases, while hiding the exact locations of observations.

As this work focuses on analysing diurnal and seasonal patterns of model biases, data only from observation campaigns that lasted longer than one year were used in the work. Observations at heights of 50 m or higher AGL were included in the analysis. In total data from 508 observation locations were included in the work, 504 of these locations provided both wind speed and direction data, while four provided only the wind speed data. Figure 3 (a) shows the distribution of observation heights. In most observation locations, the winds were measured at heights between 50 m and 125 m. However, the highest observation campaigns were conducted at heights of almost 300 m. 289 observation campaigns lasted between 1 and 2 years,

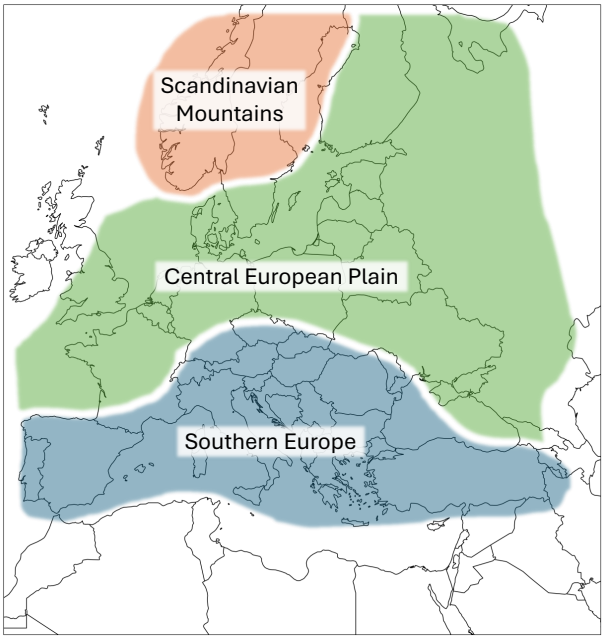

Figure 1. Map showing the geographical regions used for discussion of spatial patterns in the results.

118 campaigns lasted between 2 and 3 years, 49 campaigns lasted between 3 and 4 years, and 52 campaigns lasted 4 years and more. Most of the campaigns cover some subperiod between 2000 and 2024. Due to the different spatial and temporal coverage of the model datasets, not all observation campaigns were compared against all model datasets.

For the purposes of this work, to quantify the local complexity of the terrain around the observation locations, we use the uniformly sampled standard deviation of the terrain elevation within a 5 km radius derived from Copernicus $3''$ (3 arcsecond) DEM (digital elevation model). For brevity, it is further denoted as $SD(z)$. Figure 3 (b) shows the distribution of $SD(z)$. It can be seen that the entire range of $SD(z)$ values is well represented, including offshore locations with $SD(z) = 0$ and highly complex terrain with $SD(z)$ exceeding 200 m. Figure 4 shows spatially aggregated values of $SD(z)$ at the observation locations. It can be seen that in Central European Plain at observation locations the values of $SD(z)$ are smaller, indicating locally simpler terrain near the observation sites. Meanwhile, in Scandinavian Mountains and Southern Europe, the values of $SD(z)$ are higher, indicating locally more complex terrain near the observation sites.

Figure 5 shows the distribution of elevation differences between the model and the real-world at observation locations in all seven model datasets. The majority of the observation locations are located above the model grid-cell terrain elevation. For global reanalyses and NORA3, only approximately 28% of the observation locations are located below the model grid-cell terrain elevation. For other mesoscale model datasets, the same is true for only approximately 22% of observation locations. The magnitude of the negative differences between the model and the real-world elevation is generally greater than the magnitude of the positive ones. Depending on the model dataset, between 8% and 41% of the observation locations are located more than

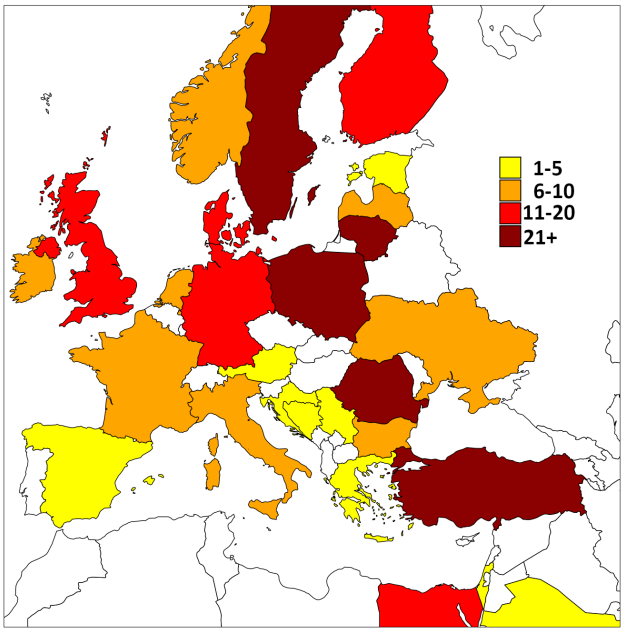

Figure 2. Region of interest and approximate number of observation locations included in the study by country. Countries are categorically coloured based on the number of observation locations included in the study. No observation data were used from countries coloured in white (including microstates).

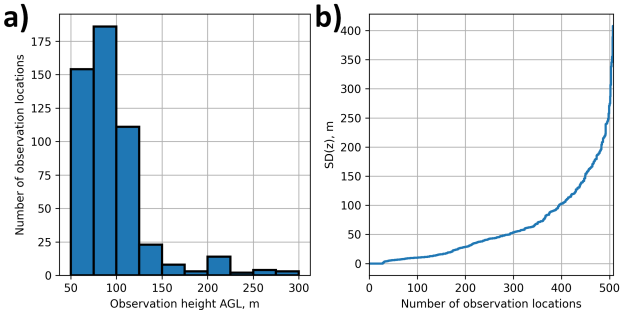

Figure 3. Information about observational dataset used in the work. (a) shows a histogram of observation heights. Left side of the bin is inclusive and right side exclusive. (b) shows ranked values of $SD(z)$ in metres for observation locations.

100 m above the model terrain elevation. On the other hand, for all models, only less than 5% of the observation locations are located more than 100 m below the model terrain elevation.

If observation locations were installed randomly inside a grid-cell, it would be expected that the distribution of the differences between the model and the real-world terrain would be symmetrical. In areas with larger $SD(z)$ these differences would be greater in magnitude. However, in case of the EMD mast database, the distribution is skewed towards locations where the

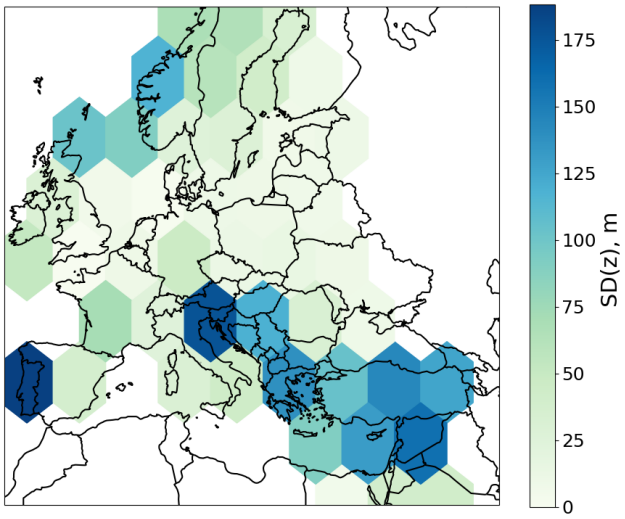

Figure 4. Map showing spatial distribution of values of $SD(z)$ at observation locations. Colour of a hexagonal bin represents the average value of $SD(z)$ between all masts located inside the bin.

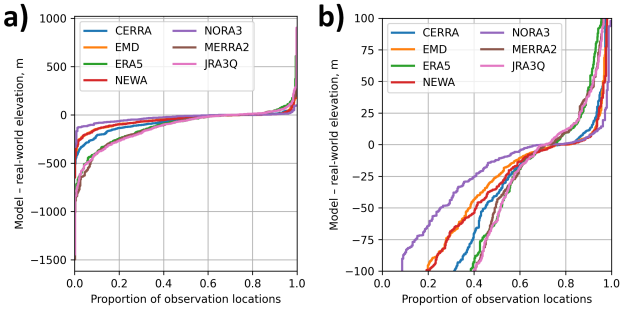

Figure 5. Empirical cumulative distribution functions of the terrain elevation difference at observation locations between model and real-world for different model datasets. (b) is a zoomed version of (a).

real-world terrain elevation is higher than the one in model. This is consistent with the idea that measurements are carried out at the potential locations of wind farms, i.e. locally windier locations that are expected to be at locally higher elevations. Moreover, in complex terrain regions, where $SD(z)$ is higher, observation locations are generally positioned higher above the model terrain elevation than in simple terrain regions. This must be taken into account when interpreting the results of this work, as wind speeds are generally higher at higher elevations locally.

The magnitude of the elevation differences appears to be related to the model grid spacing. Models with a finer grid spacing tend to show differences between the model and the real-world terrain elevation that are smaller in magnitude. All global reanalyses show similar magnitude of the elevation differences. The magnitude of the differences is smaller in CERRA (5.5 km grid spacing) and even smaller in EMD-EUR+ and NEWA (3 km grid spacing). Although NORA3 has the same resolution

as EMD-EUR+ and NEWA, it shows a significantly smaller magnitude of elevation differences, likely due to the fact that it covers only Northern Europe.

Observation data in the EMD's mast database were previously quality controlled by the individual data providers using in-house methods, making them suitable for wind resource assessment. In addition, the data were further checked for obvious errors. Obviously erroneous values were excluded: wind direction outside the range $[0°, 360°)$ and wind speed outside the range $[0, 100]$ m s^{-1}. Periods with more than three consecutive 0 m s^{-1} wind speed measurements were excluded, as those are likely to be improperly labelled missing observations.

The frequency of observations is either 1 hour or 10 minutes, depending on the particular observation campaign. On the other hand, model output is provided hourly or every three hours. Wind speeds in mesoscale models do not represent the same turbulence characteristics as the observed winds on the 10 minute timescale. To better match flow characteristics between model and observations, the observed values were averaged to the hourly resolution for comparison purposes.

2.2 Methods

2.2.1 Comparing models with observations

The bias metric was used to quantify the differences between the models and the observations. Bias is defined as the average difference between modelled and observed values. For wind energy applications, accurate predictions of the wind speed are generally assumed to be more relevant than the wind direction. However, in this work, a holistic analysis is performed and wind speed biases are considered in context with wind direction biases to seek their physical explanation.

The positive wind speed bias indicates that the model overestimates the wind speed, while the negative wind speed bias indicates that the model underestimates the wind speed. As the wind direction is a circular variable, the bias metric cannot be applied directly. To address this issue, 360°was added to the observed wind direction when necessary to ensure that the difference between the modelled and observed values is between -180°and 180°. Positive wind direction bias indicates that modelled winds are more clockwise than the observed ones, while negative wind direction bias indicates that modelled winds are more anti-clockwise than the observed ones.

We analyse spatial, diurnal, and seasonal patterns of wind speed and direction biases. For this purpose, each observation location was described by a 24×12 variables – mean differences between modelled and observed winds aggregated by the hour of day and month of the year. In the case of the JRA-3Q reanalysis, 8×12 variables were used, since it provides an output every 3 hours. Principal component analysis was applied to seek temporal and spatial patterns of model biases (described in subsubsection 2.2.2).

When comparing models with observations, it should be considered how to spatially collocate model output and observations to avoid representativeness errors. Our analysis was designed in a way to seek the connection between model biases and differences between the model terrain elevation and the actual terrain elevation. Therefore, when comparing the model with the observations, the model data from the closest horizontal grid cell to the observation campaign location were used without

considering any land properties, which is the simplest approach. Our findings can be used in future studies, when deciding which spatial collocation method between model output and observations to use.

As models generally output winds at different heights than observations, for comparison purposes, the model output was vertically interpolated to the observation height. We use a similar vertical interpolation procedure as in Solbrekke et al. (2021) for both wind speed and direction. Interpolation was performed at each model time-step independently. Wind speed was interpolated using the power law relation. The power law exponent was calculated using wind speed data u_i at the time-step i at two heights z_1 and z_2:

$$\alpha = \frac{\ln u_i(z_1) - \ln u_i(z_2)}{\ln z_1 - \ln z_2}. \tag{1}$$

Wind speed at the target height was calculated:

$$u_i(z) = u_i(z_2) \cdot \left(\frac{z}{z_2}\right)^{\alpha}. \tag{2}$$

The wind direction was interpolated considering it as a unit vector and linearly interpolating its components between two heights. If observations were performed between two adjacent model levels, the modelled winds were interpolated to the observation height between these two levels. If observations were performed above the highest model height level, the modelled winds were extrapolated to the observation height from the two highest model levels.

When interpolating wind speeds between different heights, it should be considered that models use different methodologies when calculating 10 m winds and winds at higher levels of the atmosphere. The 10 m wind speed is usually a diagnostic variable and is not modelled directly. For example, in ECMWF forecasts 10 m winds are interpolated from the lowest model level (Owens and Hewson, 2018). The roughness length of the short grass (0.03 m) which matches recommended WMO observation conditions is used instead of the actual roughness length of the model grid-cell. Therefore, the use of modelled 10 m winds should be generally avoided, when interpolating winds to higher levels.

To interpolate the wind speed to any given height, wind speed values at least at two different heights are needed. All mesoscale models provide wind data at multiple heights, covering the entire range of wind mast observation heights. Therefore, using 10 m wind speeds can be avoided. However, ERA5 provides wind speeds only on 10 m and 100 m heights, and MERRA2 provides wind speeds on 10 m and 50 m heights, which makes the use of 10 m winds unavoidable. Potential effects of using these winds on the identified model biases in ERA5 or MERRA2 are described in section 4.

2.2.2 Principal component analysis

Due to high maintenance costs, observation campaigns are usually kept as short as possible, usually being just over a year and rarely exceeding three years. While such duration is usually sufficient for decision-making regarding wind farm installation, it might not be sufficiently long to be able to identify systematic biases of models, when comparing model output to observations from an individual mast. In climate sciences, a 30 year period is usually used to define systematic weather patterns, i.e., climate normals.

The motivation of the analysis is based on the assumption that the model output differs from the real-world conditions because some physical phenomena in the model are improperly represented. Each improperly represented phenomenon contributes to the total model bias by amplifying or cancelling the effects of other phenomena. To improve future atmospheric models, it is important to decompose the total model bias into contributions from each improperly represented physical phenomenon and individually fix them.

Principal component analysis (PCA) is a statistical technique that is commonly used to identify the main patterns in large and noisy multidimensional datasets (Jolliffe, 2002). The method considers correlations between original variables and derives new variables (principal components or PC for short) that are linear combinations of the original variables. New variables are created in such a way that the first principal component (PC1) explains the maximum possible variance of the data and each subsequent principal component (i.e., PC2, PC3, ...) is uncorrelated with all previous PCs while explaining the maximum possible remaining variance of the data. Therefore, only a few of these new variables are needed to describe the main modes of variability in the dataset. The values of the principal components describe how prominent each mode is for a particular data point. The principal components can be interpreted as unit vectors that describe the axes along which the data points differ from the mean values of the dataset. The linear coefficients of each principal component are known as "loadings", which can be interpreted as the vector components. Previous work has successfully applied PCA to identify seasonal patterns of meteorological variables such as wind direction (Pogumirskis et al., 2021) or temperature and precipitation (Bethere et al., 2017).

PCA is suitable for tackling the data issues described above. Firstly, it allowed to look at biases at a single observation location in context with other locations, therefore allowing to identify biases even if only one year of observational data was available at the particular location. Secondly, PCA allowed to identify the main orthogonal modes of the dataset. These modes are acquired based purely on statistical considerations. Further numerical and statistical analysis was performed that considered the diurnal, seasonal, and spatial patterns of biases that these modes represent. Based on the analysis, we linked these statistical modes to physical phenomena.

In this work, the PCA was performed separately for each model and for wind speed and wind direction. Bias at a particular location was described by 24×12=288 (8×12=96 in the case of JRA-3Q) parameters – bias values for the particular month or hour of the day. Let us denote the bias table at a location i as X_i. By taking the average value of the tables between all observation locations, we can compute the average bias of the model — $\bar{X}$, which is also a 24×12 table. These bias tables at each observation location can be viewed as points in a 288 dimensional space centred at zero. Initially, data are defined in the canonical orthonormal basis where each of 288 unit vectors $\boldsymbol{e_j}$ has 1 at position j and 0 at the other 287 positions. By applying PCA a coordinate transformation is performed, which centres the coordinate axis at the mean bias $\bar{X}$ and rotates the unit vectors $\boldsymbol{e_j}$ so that they match the principal components as described before. After the coordinate transformation, model biases can be expressed in new coordinates where principal components (i.e., PC1, PC2, ...) are the unit vectors, "loadings" are components of these vectors, and $y_{i,j}$ are the coordinates of points in the new coordinate system (known as "values" of principal components), where i denotes the observation location and j denotes the rank of the principal component. The bias

table at a particular location i in the new coordinates can be expressed as:

$$X_i = \bar{X} + y_{i,1} \cdot PC1 + y_{i,2} \cdot PC2 + \ldots + y_{i,288} \cdot PC288. \tag{3}$$

After the PCA transformation, the loadings of principal components describe modes of differences in the temporal patterns of biases. Meanwhile, the values of the principal components correspond to observation locations and allow to identify spatial patterns of biases. Since principal components are ranked by the amount of variance they explain, the first few principal components can explain the main modes of model biases. In further analysis, it was attempted to explain the most significant principal components by some physical phenomena that are improperly represented in models.

When performing PCA an important question to consider is whether a normalisation of initial variables is needed. The choice of normalisation can have a significant impact on the results. During the analysis, we attempted to link the principal components with elevation differences between the model and the real-world. We wanted to quantify the magnitude of the effects of the elevation difference on biases depending on the time of day and year. Therefore, we chose the normalisation process that would keep the original variances and units. As wind speed and direction have different units, PCA was applied to each of them separately. Therefore, the comparison between biases was performed in absolute values, i.e., in $\mathrm{m\,s^{-1}}$ for the wind speed bias and in degrees for the wind direction bias.

As PCA in its core is an eigenvector problem, scaling of eigenvectors (principal components) and new coordinates of variables (values of principal components) is arbitrary. The standard practice of normalisation is to set the principal components as unit vectors, so that the sum of squares of loadings of each principal component is 1, and loadings are dimensionless. In that case, the values of the principal components are in $\mathrm{m\,s^{-1}}$ or degrees. However, such a normalisation approach is difficult to interpret physically, since the magnitude of those values is affected by the number of dimensions of the data, which follows from the fact that the sum of squares of loadings adds up to 1.

To provide a better physical interpretation, the values of each principal component were divided by the standard deviation of the particular principal component between observation locations, making them dimensionless. On the other hand, loadings were multiplied by the standard deviation of the particular principal component between observation locations, setting their dimension to $\mathrm{m\,s^{-1}}$ or degrees. The scaling procedure can be expressed mathematically as:

$$\widetilde{y}_{i,j} = y_{i,j} / \sigma_j, \tag{4}$$

$$\widetilde{PCj} = PCj \cdot \sigma_j, \tag{5}$$

where $y_{i,j}$ is the value of the principal component j at the i-th observation location before scaling, and $\widetilde{y}_{i,j}$ is the value after scaling. PCj are loadings of the principal component j before scaling and $\widetilde{PCj}$ are loadings of the principal component j after scaling. σ_j is the standard deviation of the values of the principal component j:

$$\sigma_j = \sqrt{\frac{1}{n-1} \sum_{i=1}^{n} (y_{i,j} - \bar{y}_j)^2}. \tag{6}$$

After normalisation is applied, the value of the principal component describes the prominence of the bias described by that principal component at a particular location. The standard deviation is chosen as an interpretable measure, since in the case of the normal distribution 99.7 % of the data lie within 3 standard deviations of the mean. On the other hand, loadings describe a characteristic magnitude of the bias in the dataset — the magnitude of the bias at a location where the value of a principal component is 1 standard deviation from the mean.

2.2.3 Terrain influence on biases

Previous studies have identified that synoptic scale and mesoscale models show stronger wind speed biases in complex terrain. This work attempts to provide a physical explanation for the negative wind speed bias on hilltops and the positive wind speed bias in valleys. Our hypothesis is that wind speed biases in complex terrain are due to the terrain elevation mismatch between the model and the real-world. The terrain in models is spatially aggregated, and it is a smoothed version of the real-world terrain. For points that are locally at a higher elevation, i.e., hilltops, smoothing of the terrain generally decreases the elevation. It not only decreases the absolute elevation of the hilltop, but also decreases the height of the hill relative to its surroundings. Meanwhile, for points that are locally at a lower elevation, i.e., valleys, smoothing generally increases the elevation. It not only increases the absolute elevation of the valley, but also decreases the depth of the valley relative to its surroundings. In addition, smoothing of the terrain generally decreases the magnitude of terrain slopes and decreases the variability of the resolved terrain, decreasing the orographic drag.

We use elevation differences between the model and real-world terrain as a statistical explanatory variable for model biases. Based on physical considerations, the elevation difference can potentially explain model biases. For example, if a model underestimates the height of the hill, it would underestimate the orographic speed-up caused by the hill. Moreover, the elevation difference between model and real-world is a variable that can be easily modified in the input data or accounted for when post-processing model output to potentially fix model biases. The elevation difference does not directly describe changes in slopes or resolved orographic drag. However, a larger absolute elevation difference would indicate stronger changes in the terrain locally due to smoothing, indicating a stronger reduction in slopes and orographic drag due to reduced terrain variability.

In this work, we attempted to explain model biases by the terrain elevation difference between models and the real-world. We wanted to ensure that the relationship between bias and elevation difference appears in the data without a priori imposing it. Moreover, we wanted to ensure that the statistical explanatory power of the elevation difference is stronger than the established result that models generally show stronger wind biases in complex terrain, i.e., at higher elevations. Therefore, we analysed how well model bias statistically can be explained by the difference between the model and real-world elevation versus the case where only the real-world elevation is considered. For such purpose we performed stepwise linear regression. In the first case, only the real-world elevation was used to linearly predict values of the principal component of model bias. In the second case, both the model and the real-word elevation were considered as predictors. The F-test was used to evaluate whether the increase in correlation is significant when both the model and the real-world elevation is used to explain the model biases versus the case when only the real-world elevation is used as the explanatory variable. In all cases, the regression coefficients for the real-world and model terrain had approximately the same magnitude and opposite signs, indicating that bias is explained by

their difference. In further work, the linear combination of model elevation and real-world elevation, which predicts model biases using the linear regression, is referred to as the "weighted difference between model and real-world elevation".

Model biases can be caused not only by the smoothing of the terrain, but also by errors in the terrain datasets themselves. For example, Gelaro et al. (2017) has reported that MERRA reanalysis used an outdated terrain source compared to MERRA2 reanalysis, which contained large terrain biases of up to 600 m in Greenland. These errors in terrain representation have significantly affected the modelled surface mass balance in Greenland between these two reanalyses.

Digital terrain models (DTM) are datasets that provide spatially gridded terrain elevation data. On the other hand, digital elevation models (DEM), which are used in this study, also consider other objects on the Earths surface, such as trees and buildings, in their elevation data. All mesoscale model datasets analysed in this work used the GMTED2010 elevation dataset (Danielson and Gesch, 2011), which compiles terrain data from 11 different source DEMs. ERA5 uses its own elevation dataset that is compiled from 5 different source DEMs (ECMWF, 2016). To the authors knowledge, the terrain elevation source data for MERRA2 and JRA-3Q are not publicly disclosed. For the region of interest, both ERA5 and GMTED2010 use SRTM data south of $60°N$, which was collected in 2000. North of $60°N$ ERA5 uses GLOBE data, which was made publicly available in 1999, while GMTED2010 uses DTED1 data, which was collected in 2000. While the quality assessment of the elevation datasets themselves is out of the scope of this study, we acknowledge that wind biases can be influenced by errors in terrain datasets. Therefore, as a source for the real-world terrain, we use data from Copernicus $3''$ ($\approx$90 m in latitudinal direction) DEMs. Data in Copernicus DEM have been collected between 2011 and 2015, and it has shown better accuracy than older DEMs (Meadows et al., 2024). The absolute vertical accuracy of GMTED2010 at 90% confidence level is 10 m (Danielson and Gesch, 2011), while for Copernicus DEM it is 4 m (Fahrland, 2022).

It has to be kept in mind that both wind and elevation data from global reanalyses are provided regridded to the orthogonal latitude-longitude grid.

This work focuses on identifying local model biases that are directly influenced by terrain differences. In other words, model bias at a particular grid-point is present because the elevation of a grid-cell is different from the terrain elevation at the observation location. These effects can be identified by considering the correlation of model bias and elevation difference between the model and the real-world. However, mountains can influence the wind field tens to hundreds of kilometres downstream (Draxl et al., 2021). Therefore, local differences in terrain elevation between the models and the real-world can theoretically cause wind biases further away. Identifying these biases is outside the scope of this work.

2.2.4 WRF modelling

The results of the comparison between models and observations suggested that the terrain height difference between models and the real-world has a significant effect on the differences between the modelled and observed winds. To test whether the modelled winds can be adjusted in a controlled manner by adjusting the model terrain elevation, we performed two one-year WRF model simulations using different terrain source datasets, but otherwise the same setup. One run used GMTED2010 terrain input data at $30''$ ($\approx$900 m in latitudinal direction) resolution, while the other used $5'$ (5 arcminute) ($\approx$9 km in latitudinal direction)

resolution. GMTED2010 is the default terrain dataset provided with the WRF model installation at different resolutions. The motivation for using these two terrain datasets to test the hypothesis lies in how the terrain is represented at different resolutions.

In the real-world, terrain height is a continuous variable, i.e., its resolution is infinitely fine. In the Copernicus dataset used in this work, the terrain is aggregated on a $3''$ grid ($\approx$90 m in latitudinal direction). In the WRF model run that uses $30''$ terrain input data, the terrain is aggregated on a 3 km grid, since the model grid is coarser than the input data. Meanwhile, in the WRF model run that uses $5'$ input data, the terrain is smoothed, since the input terrain resolution is coarser than the model resolution.

When observations are compared with the 3 km model, the flow over the real-world terrain is compared with the flow over the 3 km terrain, which is a smoothed version of the real-world terrain. Similarly, when modelled winds over the $30''$ terrain are compared with modelled winds over the $5'$ terrain, the flow over a detailed terrain is compared with the flow over a smoothed version of the same terrain. An illustrative example of a topographic profile in the Copernicus dataset as well as both WRF models is shown in Figure 6. It can be seen that in the Copernicus $3''$ DEM hills are generally higher and valleys are generally deeper than in WRF model that uses $30''$ terrain input. Similarly, in the WRF model that uses $30''$ terrain input hills are generally higher and valleys are generally deeper than in the WRF model that uses $5'$ terrain input.

Models and observations generally show differences due to numerous factors. On the other hand, the two models used in this work differ only by their terrain. Therefore, their differences are caused solely by differences in terrain representation. The model that uses $30''$ terrain is used as an analogy for the flow in the real world, i.e., with fully resolved terrain. On the other hand, the model that uses $5'$ terrain is used as an analogy for the flow in a model, i.e., with an aggregated and smoothed terrain. It is hypothesised that terrain smoothing differences between these two models would induce differences in modelled winds similar to the ones that exist between a model and observations. When comparing models with observations, observed winds were subtracted from the modelled winds. The order in which models were subtracted was chosen to represent the same effects as when comparing models and observations. The output of the $30''$ terrain model was subtracted from the output of the $5'$ terrain model. It should be noted that the WRF setup in our experiments did not use any subgrid terrain properties, e.g. subgrid terrain variance, as an input. Even if we used a WRF setup that considers subgrid terrain properties, in WRF these are not dynamically derived from the input terrain dataset, but are pre-calculated on a grid. Therefore, changing only the terrain input dataset in the WRF model would not directly affect subgrid terrain properties.

Both WRF model runs were performed on a 810×1620 km domain covering Sweden, consisting of 270×540 grid cells. To avoid domain boundary effects of the low resolution boundary conditions, 10 outer grid cells of both domains were excluded from the comparison. Model domains, and differences in their terrain are shown in Figure 7. The average difference between elevations in both models is 0.4 m, the maximum absolute difference is 490.2 m, and the standard deviation of differences is 35.6 m. Both models used otherwise the same WRF model setup described in Table A1. Hourly winds at 100 m height AGL were used for comparison, since they are close to the typical observation height for the EMD mast database. The analysis was performed using PCA in a similar manner as that applied when comparing models with observations: each of the model grid-points was described by 24×12 variables – average differences in mean wind speed or direction between models for the particular hour of the day or month of the year.

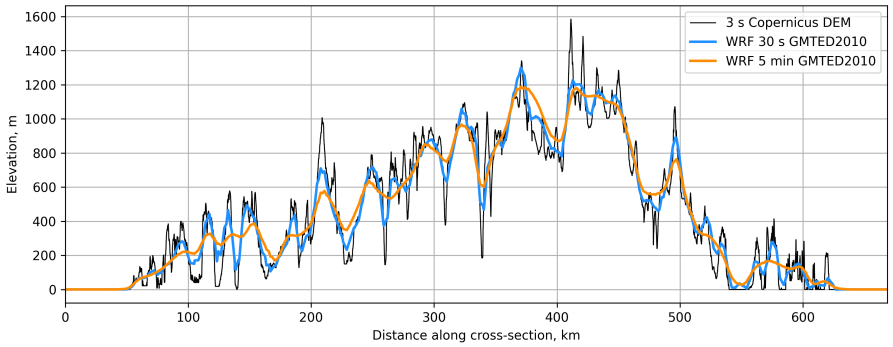

Figure 6. An example of a topographic profile in Copernicus $3''$ DEM and both WRF models used in this work. The exact location of the line is shown on the map in Figure 7. Terrain elevation in metres is shown on the y axis and distance along the line in kilometres is shown on the x axis.

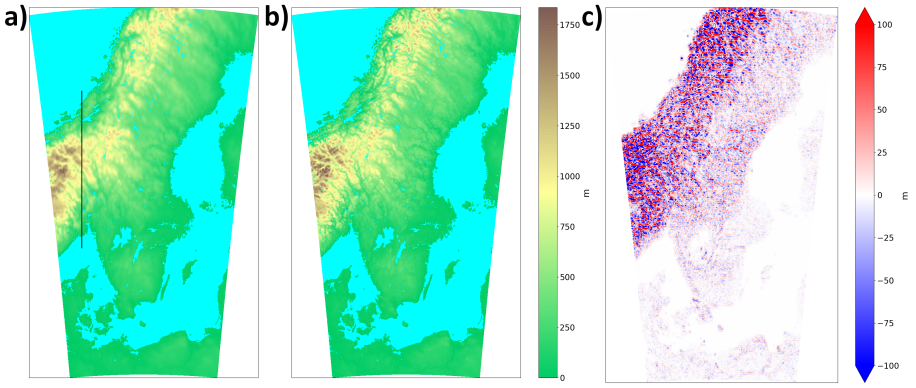

Figure 7. Terrain elevation height in metres and domain extent for both WRF model runs (including the buffer zone). (a) terrain using $5'$ resolution input data, (b) terrain using $30''$ resolution input data and their difference (c). The line of the topographic profile from Figure 6 is included.

Sweden was chosen as the simulated region due to several factors. First, choosing all of Europe as a domain would significantly increase the computational time. Second, Sweden has a diverse terrain — complex terrain in the north and simple terrain in the south. Moreover, large areas of open sea are present. Third, the EMD mast database has a high observation coverage of the Sweden, which allowed to compare these model runs against observations for future work. Due to the higher availability of observation data, 2011 was chosen as the year for both runs.

3 Results

3.1 Comparison between models and observations

The results of the principal component analysis suggest that all seven models show similar principal spatial and temporal patterns of the wind speed and direction biases. Temporal patterns of biases in the Central European Plain differ significantly from patterns in mountainous regions — Southern Europe and Scandinavian Mountains. Values of PC1 of wind speed bias and values of PC2 of wind direction bias show similar spatial patterns in all seven models. However, for brevity, detailed results only for the ERA5 reanalysis are presented in the main part of the paper. For other model datasets, mean biases and loadings of principal components are included in the Appendix B.

The temporal patterns of the spatially averaged wind speed bias show differences depending on the dataset. In ERA5 (Figure 10, (b)) and MERRA2 the average wind speed bias is more positive during the day and more negative during the night. In NORA3, EMD-EUR+, CERRA, NEWA and JRA-3Q the average wind speed bias is more positive during the winter and more negative during the summer. In NORA3, EMD-EUR+, CERRA, and JRA-3Q the bias is more negative during the day and more positive during sunrise and sunset. In NEWA the wind speed bias is more negative during the day, and the magnitude of the bias is significantly higher than in other models. However, NEWA shows a more positive bias only during sunset and does not show a more positive bias during sunrise.

The principal components describe the modes how the temporal patterns of model biases in different observation locations differ from the temporal pattern of the spatially averaged model bias. For example, the temporal patterns of spatially averaged wind speed bias in ERA5 are shown in (Figure 10, (b)). The loadings of PC1 of the wind speed bias in ERA5 are shown in Figure 9, (a). The temporal patterns of wind speed bias at a particular location can be calculated by combining the spatially averaged temporal pattern of the model wind speed bias with the sum of the values of all principal components at that location, each multiplied by the corresponding principal component. PCA is performed with the goal of linking each principal component to some improperly represented atmospheric phenomena. By setting the values of all principal components except one to zero, it is possible to analyse how model biases in different regions are affected by the improper representation of a particular atmospheric phenomenon. Further in the work PC1 of the wind speed bias (explains 82.5 % of variance in the wind speed bias in the ERA5 reanalysis) and PC1 and PC2 of the wind direction bias (explain 61.1 % and 5.7 % of variance in the wind direction bias in the ERA5 reanalysis, respectively) are analysed. For other models, PC1 of the wind speed bias explains between 61.6 % and 81.3 % of variance, PC1 of the wind direction bias explains between 52.4 % and 68.3 % of variance, and PC2 of the wind direction bias explains between 3.4 % and 6.3 % of variance.

Figure 8 shows spatial patterns of PC1 values of the wind speed bias. More positive PC1 values are present at observation sites in the Central European Plain. Meanwhile, more negative PC1 values are present at observation sites in mountainous regions – Scandinavian Mountains and Southern Europe. It indicates that the temporal patterns of the wind speed biases generally differ between these regions. Characteristic temporal patterns of biases for regions with positive (negative) values of PC1 can be calculated by taking PC1 multiplied by the standard deviation of PC1 values between all observation locations and adding (subtracting) it to (from) the spatial averaged table of biases.

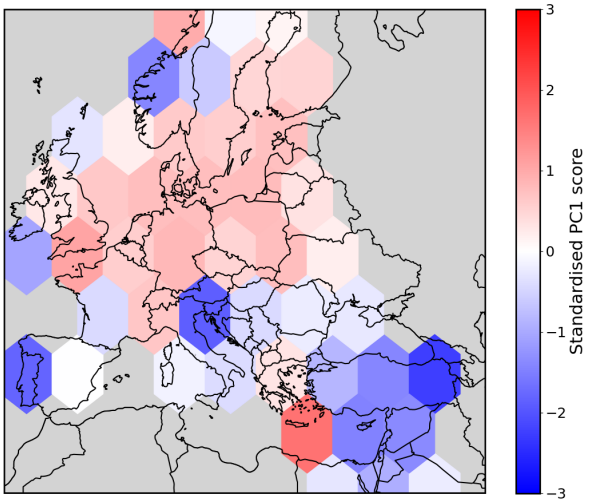

Figure 8. Map showing spatial distribution of values of the PC1 of the wind speed bias in ERA5 reanalysis. Colour of a hexagonal bin represents the average value of PC1 between all masts located inside the bin. Values are normalised by dividing a value of PC1 at each location by the standard deviation of all PC1 values between all observation locations.

In mountainous regions, the values of PC1 of the wind speed bias are more negative. Therefore, if we subtract PC1 of the wind speed bias multiplied by the standard deviation of values of PC1 between all observation sites from the average bias table, we obtain a characteristic bias table for mountainous regions (Figure 10, (a)). It can be seen that in mountainous regions, all models show an overall more negative wind speed bias. Wind speed bias is more positive during the day and more negative during the night.

In the Central European Plain, the values of PC1 of the wind speed bias are more positive. Therefore, if we add PC1 of the wind speed bias multiplied by the standard deviation of the PC1 values between all observation sites to the average bias table, we obtain a characteristic bias table for the Central European Plain (Figure 10, (c)). It can be seen that in Central European Plain the bias is more positive during winter than during summer and more negative during the day than during the night.

Temporal patterns of spatially averaged wind direction bias show differences depending on the dataset. In EMD-EUR+, CERRA, ERA5 (Figure 12, (b)) and MERRA2 the wind direction bias is more clockwise during the day and more anti-clockwise during the night. In NORA3 wind direction bias is more clockwise in winter and more anti-clockwise in summer. In NEWA the wind direction bias is more clockwise during the night and more anti-clockwise during the day. In JRA-3Q the wind direction bias is more clockwise closer to sunset.

Similarly to values of PC1 of the wind speed bias, the values of PC2 of the wind direction bias show differences between parts of Europe – Central European Plain and mountainous regions (Figure 11). The difference is that the sign of PC2 of the wind direction bias is the opposite to the sign of PC1 of the wind speed bias. That is, values of PC2 of the wind direction bias are negative at the observation sites in the Central European Plain and positive at the observation sites in the mountainous regions. Characteristic patterns of the wind direction biases for these regions can be acquired by adding (subtracting) loadings

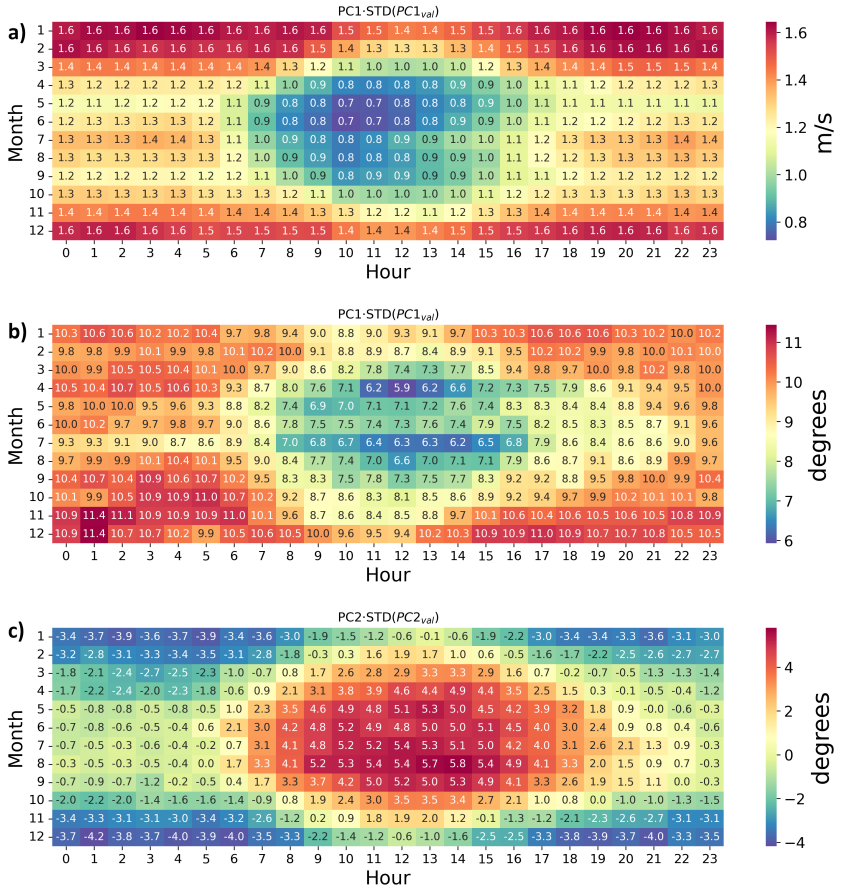

Figure 9. ERA5 reanalysis and observation comparison. Loadings of the PC1 for wind speed bias (a), PC1 of wind direction bias (b) and PC2 of wind direction bias (c). Loadings are normalised by multiplying them by the standard deviation of values of the particular principal component between all observation locations. Units are m s^{-1} for wind speed and degrees for wind direction.

of PC2 of the wind direction (Figure 9, (c)) multiplied by the standard deviation of PC2 values between all observation sites to (from) the spatially averaged temporal pattern of the wind direction bias. In the Central European Plain, the values of PC2 of wind direction bias are negative. Therefore, in the Central European Plain, the temporal patterns of the wind direction bias are closer to the ones shown in Figure 13, (a). In the Central European Plain, all models show more clockwise wind direction bias in winter and more anticlockwise wind direction bias in summer. In mountainous regions PC2 of the wind direction bias shows positive values. Therefore, in mountainous regions the characteristic temporal patterns of the wind direction bias are closer to the ones shown in Figure 13, (c). In mountainous regions, the wind direction bias is more clockwise during the day and more anticlockwise during the night. PC2 of the wind direction bias describes only differences in the temporal patterns of the wind direction bias, while PC1 of the wind speed bias describes both differences in temporal patterns and the overall magnitude of the bias (more positive or negative wind speed bias).

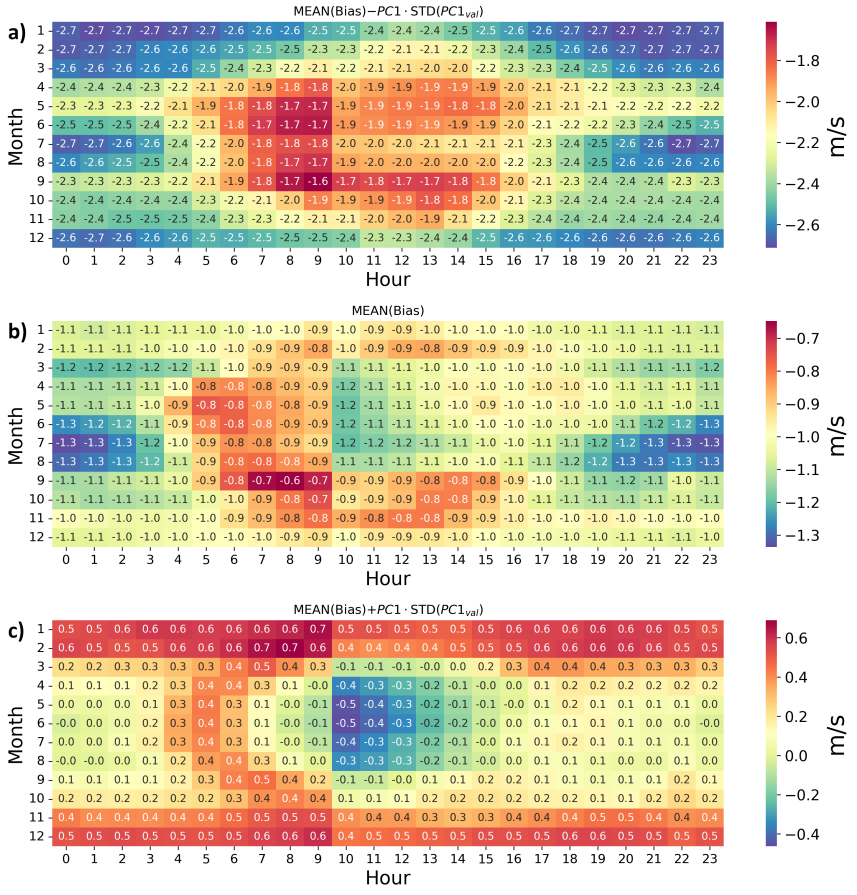

Figure 10. Wind speed biases (in $\mathrm{m\,s^{-1}}$) in ERA5 reanalysis dependent on month (y axis) and time of day (x axis). Spatially averaged bias is shown in (b). (c) shows spatially averaged bias plus 1 standard deviation of values of the PC1 between observation locations. (a) shows spatially averaged bias minus 1 standard deviation of values of the PC1 between observation locations.

The overall magnitude of the wind direction bias (overall clockwise or anticlockwise wind direction bias) is described by the PC1 of the wind direction bias. The loadings of PC1 of the wind direction bias are shown in Figure 9. Positive values of PC1 of the wind direction indicate that wind direction bias at a particular location is overall more clockwise, while negative values indicate that the bias is overall more anticlockwise. The loadings of PC1 of the wind direction bias are different for different months and times of the day. However, when adding (Figure 12, (c)) or subtracting (Figure 12, (a)) 1 standard deviation of values of PC1 of the wind direction bias to the spatially averaged wind direction bias has a much smaller effect on temporal patterns than in the case for PC1 of the wind speed bias and PC2 of the wind direction bias.

All models show similar spatial patterns of values of PC1 of the wind direction bias. However, in contrast to PC1 of the wind speed bias and PC2 of the wind direction bias, values of PC1 of the wind direction bias shows no clear spatial patterns (cannot be shown due to confidentiality reasons). Values of PC1 in the same model can differ significantly even when two

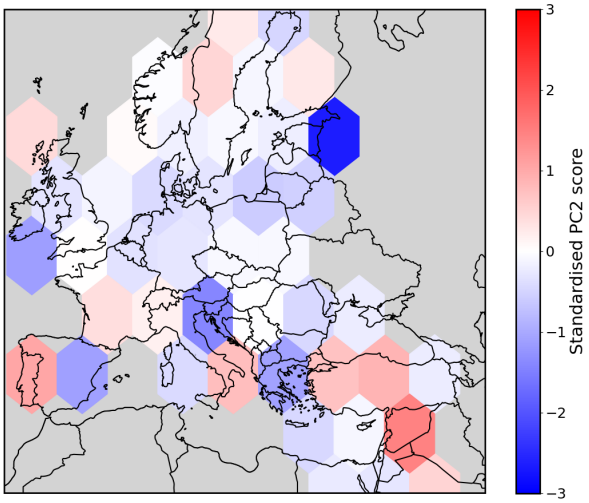

Figure 11. Map showing spatial distribution of values of the PC2 of the wind direction bias in ERA5 reanalysis. Colour of a hexagonal bin represents the average value of PC2 between all masts located inside the bin. Values are normalised by dividing a value of PC2 at each location by the standard deviation of all PC2 values between all observation locations.

observation points are located within the same model grid-cell and in a simple terrain. The standard deviation of the average wind direction bias between observation locations ranges between 8 and 10 degrees depending on the model. The magnitude of the bias differs only slightly depending on the model, while the elevation differences from the real-world in mesoscale models are more than two times lower in magnitude than for global reanalyses, which indicates that PC1 of the wind direction bias cannot be significantly explained by the elevation differences. Nevertheless, in Figure 14 it can be seen that the elevation differences show a weak explanatory signal in the values of PC1, showing a weak but statistically significant correlation of approximately 0.2 in most models.

According to Möhrlen et al. (2022) a wind direction measurement bias of 5° is acceptable for the wind resource assessment, which is significantly lower than the one observed in our dataset. Jiménez and Dudhia (2013) compared the observed and modelled winds at 2 km resolution over Iberian peninsula. They have observed biases in mean wind direction on the order of tens of degrees. Significantly stronger wind direction biases were present in complex terrain, which could be only partially mitigated by choosing a more representative nearby grid-point. They explained these biases by models being unable to sufficiently well represent local terrain features using a 2 km resolution.

Since in our dataset strong wind direction biases were also present in a simple terrain, it suggests that the mean wind direction bias is likely a combination of measurement biases, biases induced by the local unresolved terrain features, biases caused by the elevation discrepancy between models and the real-world, and possibly biases caused by other physical processes that were not considered in this work. Identifying exact causes of wind direction biases at each observation location would require manual inspection of the surroundings of each observation location. As our analysis focuses on identifying patterns of biases on a larger scale, manual individual inspection of the observation sites is outside the scope of this study.

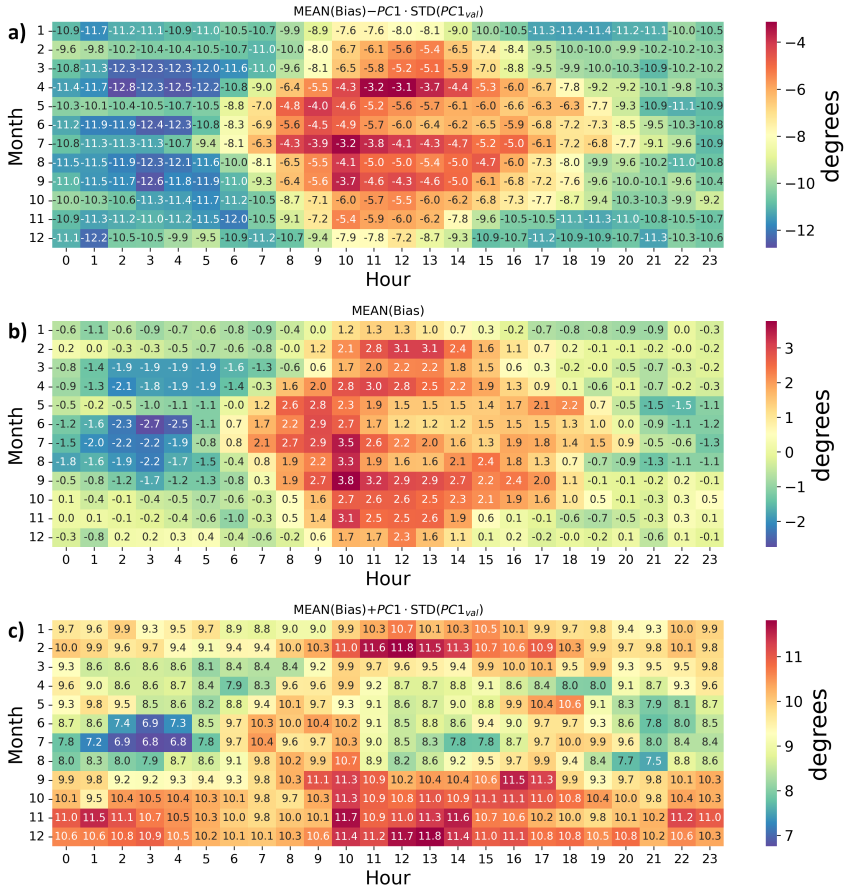

Figure 12. Wind direction biases (in degrees) in the ERA5 reanalysis dependent on month (y axis) and time of day (x axis). Spatially averaged bias is shown in (b). (c) shows spatially averaged bias plus 1 standard deviation of values of the PC1 between observation locations. (a) shows spatially averaged bias minus 1 standard deviation of values of the PC1 between observation locations.

To test the hypothesis of whether the biases are induced by the differences in the terrain elevation between models and real-word, correlations between principal components and terrain variables – real-world elevation, model elevation and their weighted difference were considered. The correlations between elevation variables and the principal components of wind speed and direction biases are summarised in Figure 14. Since the sign of principal components is arbitrary when applying PCA to different model datasets, correlations are multiplied by -1 when necessary to match the sign with the ERA5 as was presented above. For all models and all bias variables, it can be seen that the correlation becomes noticeably stronger when the elevation difference is considered, compared to a case where only the real-world elevation is considered. The results of the F-test show that the increase in correlation is statistically significant in all cases at the significance level of 0.05.

While correlations between elevation difference and bias variables are statistically significant, in some cases they are weak and cannot be used to provide a hypothesis about a potential physical cause. However, it has to be kept in mind that the

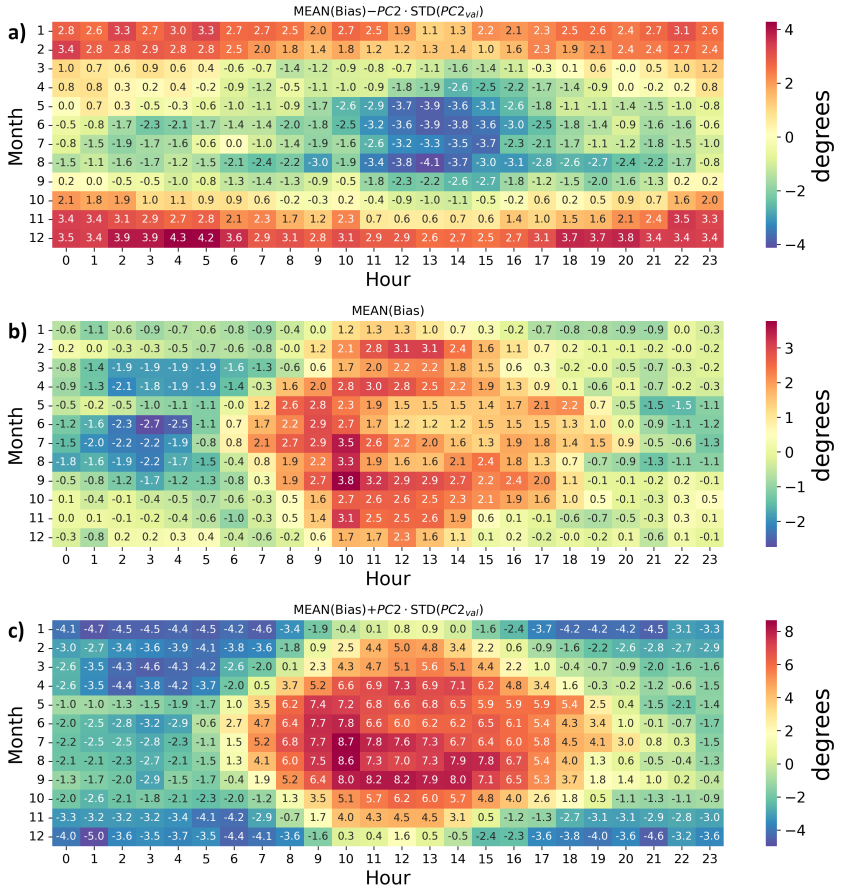

Figure 13. Wind direction biases (in degrees) in the ERA5 reanalysis dependent on month (y axis) and time of day (x axis). Spatially averaged bias is shown in (b). (c) shows spatially averaged bias plus 1 standard deviation of values of the PC2 between observation locations. (a) shows spatially averaged bias minus 1 standard deviation of values of the PC1 between observation locations.

atmosphere is chaotic and model biases are caused by a lot of different physical phenomena. Therefore, if the fact of causation can be established, low correlation implies presence of noise in the data. In that case, correlation is used to measure the strength of the effect rather than to indicate the potential presence of the effect. For example, a correlation (R) of 0.3 between bias and elevation difference indicates that elevation difference explains 9 % of the variance (R^2) in model biases. The numerical experiment that establishes the link how changing the elevation changes the modelled winds is described in subsection 3.2. In section 4, it is described which physical phenomena might theoretically cause wind biases in the case when the model elevation differs from the real-world elevation.

The ERA5 reanalysis shows the strongest correlations between elevation difference and bias variables. The correlation is 0.71 for values of PC1 of the wind speed bias and 0.41 and -0.50 for values of PC1 and PC2 of the wind direction bias, respectively. In case of wind speed, the effects of the elevation difference of the mean bias and temporal patterns of biases

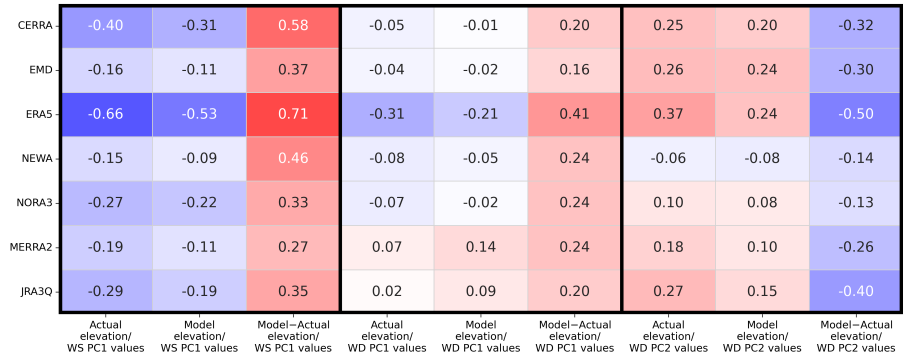

Figure 14. Correlations between values of principal components that describe model biases and terrain variables (x axis) for different model datasets (y axis). WS denotes wind speed and WD denotes wind direction biases.

are combined into PC1. Meanwhile, in case of the wind direction bias, the effects of the elevation difference are split between PC1 for the mean bias and PC2 for temporal patterns of bias. When the elevation difference is considered, EMD-EUR+ and NEWA show the strongest increases in the correlation versus the case when only real-world elevation is considered. For PC1 of the wind speed bias, the correlation with real-world elevation is only -0.16 for EMD-EUR+ and -0.15 for NEWA. However, when the elevation difference is considered, the correlation increases to 0.37 and 0.46 respectively. The correlations between real-world and model elevation are 0.93–0.94 for global reanalyses and 0.98–0.99 for mesoscale model datasets.

All correlations between the principal components of model biases and weighted elevation differences between model and real-world are statistically significant at the significance level of 0.05. The smallest number of masts was used when assessing biases in the NORA3 dataset, only 254. For 254 data points, the correlation coefficient with an absolute value greater than 0.12 is statistically significant at the significance level of 0.05. For other datasets, the correlation threshold is even lower. When the model elevation or the real-world elevation is considered individually, the correlation is not always statistically significant.

These correlations suggest a statistical relationship between model wind biases and the elevation difference between models and the real-world. If observations are performed above the model grid-cell elevation, then models shows a tendency to underestimate the wind speed. The underestimation is stronger in winter than in summer and stronger during the night than during the day. Additionally, the model shows an overall anti-clockwise wind direction bias. The bias is more anti-clockwise in winter than in summer and more anti-clockwise during the night than during the day. On the other hand, if observations are performed below the model grid-cell elevation, then models show tendency to overestimate the wind speed. The overestimation is stronger in winter than in summer and stronger during the night than during the day. Additionally, the model shows an overall clockwise wind direction bias. The bias is more clockwise in winter than in summer and more clockwise during the night than during the day.

3.1.1 100 m wind speed bias in ERA5

One of the objectives of the work was to assess how the 100 m wind speed bias from ERA5 is inherited in downscaled mesoscale models. In Figure 10 it is clearly visible that there is a sharp decrease in the wind speed bias from 9:00 UTC to 10:00 UTC in the ERA5 reanalysis. The decrease is also visible in the data from the CERRA reanalysis. However, it is less prominent. Meanwhile, there is no noticeable unrealistic change in the wind speed bias between 9:00 and 10:00 UTC in the plots for NORA3, NEWA, and EMD-EUR+.

The prominence of 100 m wind speed bias in the mesoscale model output can be explained by model initialisation strategies. CERRA reanalysis assimilates observations every three hours, and in this work data with a spin-up time of only one hour are used. Moreover, both CERRA and ERA5 are developed by the same organisation ECMWF. Therefore, the CERRA reanalysis is likely to be closer to the host reanalysis ERA5 than other downscaled products.

The NORA3 dataset uses a longer spin-up time of 3 hours than CERRA, which is likely to reduce the effect of bias. NEWA and EMD-EUR+ reinitialise model once a week. Moreover, they are always initialised at 0:00 UTC, during the 21:00–9:00 UTC assimilation window, which does not experience 100 m wind speed issues in the ERA5. Therefore, these models are less affected by the issue. However, it has to be kept in mind that all mesoscale models use boundary conditions from ERA5, which are regularly updated. In addition, NEWA and EMD-EUR+ are nudged towards ERA5. Therefore, they are likely to experience a performance drop due to the 100 m wind speed issue with ERA5, despite the issue not being directly observable in the plots of this work.

3.2 WRF model comparison

The results of the model comparison with observations showed that wind speed and direction biases are correlated with the elevation difference between the models and the real-world. Moreover, the magnitude of the bias depends on the time of day and year. As model terrain elevation is something that can be easily changed in models, we made a hypothesis that the bias can be potentially improved if the model terrain is adjusted to match the real world terrain better.

To test the hypothesis, we performed an experiment by running two numerical models with different terrain input datasets and comparing their modelled winds. The goal of the experiment was to identify how the diurnal and seasonal patterns of the modelled winds change when the terrain is smoothed in the model. We anticipated that the main mode of wind differences between models with $5'$ and $30''$ input terrain resolution would be similar to the main mode of differences between modelled and observed winds. It would indicate that by adjusting terrain elevation in model it is possible to adjust modelled winds in a way that would reduce the bias caused by the elevation discrepancy.

While there might be a potential to reduce the model bias caused by the elevation discrepancy, by adjusting the model elevation, it is unclear how it would affect the overall model performance. Smoothing of the terrain affects both slopes and the resolved orographic drag caused by the terrain variability, both of which are only indirectly covered by our analysis. Moreover, in models, the terrain is smoothed for practical reasons – to reduce strong elevation gradients, which might cause numerical instabilities.

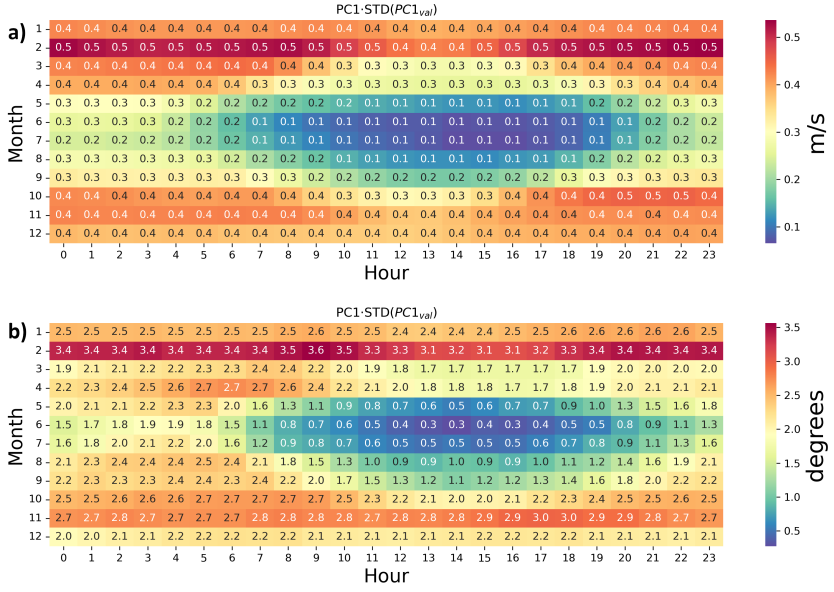

Figure 15. Model difference comparison. Loadings of the PC1 for wind speed difference (a) and wind direction difference (b) multiplied by the standard deviation of the PC1 values between all grid-points. Units are m s^{-1} for wind speed and degrees for wind direction.

When comparing two models, PCA was applied in a similar way as it was applied when comparing models and observations. However, instead of using only 508 observation locations, model differences were compared in all 250×520 grid-cells.

The loadings for the PCA of the model comparison are shown in Figure 15. The loadings of PC1 of the wind speed difference when comparing two models show similar diurnal and seasonal patterns as the loadings of PC1 of the wind speed when comparing models with observations (Figure 9). In case for wind direction difference, there is a difference from the case when comparing models with observations. When comparing models with observations PC1 describes the overall magnitude of the wind direction bias and PC2 describes diurnal and seasonal patterns of the wind direction bias. In case of comparing two models, the loadings of PC1 of the wind direction difference show similarities to the case with the wind speed. PC1 of the wind direction difference between models describes both the overall magnitude and the temporal patterns of the wind direction difference. A potential explanation of such difference is that when comparing two models there is no overall wind direction bias caused by improper reference direction calibration or subgrid obstacles.

For both wind speed and wind direction differences, values of PC1 show similar spatial patterns (Figure 16). PC1 shows slightly negative values over the sea and in Southern Sweden, where the terrain is simple. In northern parts of Sweden, where the terrain is complex, PC1 shows a high contrast in values: strongly positive and strongly negative. The patterns of these values follow the terrain. Strongly positive values are present in valleys, while strongly negative values are present on top of hills.

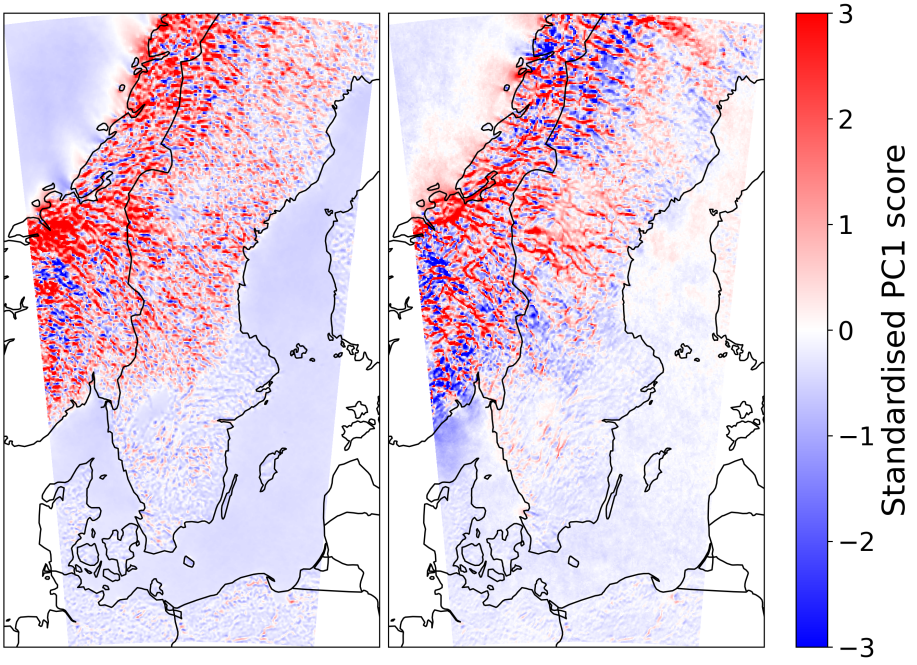

Figure 16. Values of PC1 for model differences of wind speed bias (left) and wind direction bias (right). Values are normalised by dividing a value of PC1 at each grid-point by the standard deviation of all PC1 values between all grid-points.

PC1 of the wind speed difference explains 75 % of the variance in wind speed differences between both WRF models. PC1 of the wind direction difference explains 22 % of the variance in wind direction differences between both WRF model simulations.

Similarly to observations, the principal components of the differences between two models show correlations with the elevation difference between these two models. Values of PC1 of the wind speed difference between models shows a 0.35 correlation with the elevation in $30''$ model and 0.42 correlation with the elevation in $5'$ model. When the weighted difference between elevations is considered, the correlation increases to 0.69. Values of PC1 of the wind direction difference between models shows a 0.05 correlation with the elevation in $30''$ model and 0.12 correlation with the elevation in $5'$ model. When weighted difference between elevations is considered, the correlation increases to 0.56. The correlation between elevation in the $30''$ model and the $5'$ model is greater than 0.99.

These correlations suggest that there is a similar statistical relationship between elevation differences and wind differences when two models are compared, as when models are compared with observations. If the terrain elevation of a grid-cell in two models is the same, then models on average show small differences in wind speeds and wind directions. On the other hand, if the terrain elevation of a grid-cell differs between two models, the model in which the elevation is higher on average shows a higher wind speed and a more clockwise wind direction. The wind speed difference is higher in winter than in summer and

higher during the night than during the day. The difference in wind direction is more clockwise in winter than in summer and more clockwise during the night than during the day.

By multiplying regression coefficients when explaining the bias with the elevation difference by the loadings of the principal components, it is possible to estimate the magnitude of the bias induced by the elevation difference. The elevation difference of 100 m between two models induces a difference in wind speed between 0.1 $\mathrm{m\,s^{-1}}$ in summer during the day and 0.9 $\mathrm{m\,s^{-1}}$ in winter. When comparing models with observations, the elevation difference showed an effect on the wind speed bias of approximately the same magnitude. The elevation difference of 100 m creates a difference in the wind direction between 0.4°in summer during the day and 5.6°in winter. However, the effects of the elevation difference on the wind direction bias cannot be clearly isolated from the observations since there is a large contribution to the wind direction bias from improper reference direction calibration or obstacles in the near proximity of the observation location. It is likely that the magnitude of the effect is similar as in the case when comparing two models. It should be noted that the magnitude of the effect of elevation on the modelled wind speed is averaged for the entire region and does not consider land use or any other factors.

While loadings of main principal components and correlations with terrain for model comparison and model-observation comparison look similar, spatial patterns of values of principal components on the first glance look different. When comparing models and observations, values of PC1 of the wind speed bias are more positive in simple terrain and more negative in complex terrain. On the other hand, when comparing two models, the values of PC1 of the wind speed difference are more negative on top of the hills, more positive inside valleys, and closer to zero in simple terrain. However, differences in spatial patterns of the values of principal components can be explained if we consider the fact that observation campaigns in our dataset are more often performed on top of the hills. As observation campaigns are more likely to be performed on top of the hill, the strongly negative values of PC1 of the wind speed bias are more abundant than strongly positive values when comparing models to observations in the complex terrain. This explains more negative values of PC1 of wind speed bias in complex terrain in observations.

4 Discussion

Differences in model biases between parts of Europe have been observed before in the NEWA and ERA5 model datasets (Dörenkämper et al., 2020). They have shown that wind speed biases in Europe become more positive towards the north and more negative towards the east. Previous studies have identified that both the MERRA and MERRA2 reanalyses underestimate wind speeds in Northern and Southern Europe, while overestimating wind speeds in Central Europe (Staffell and Pfenninger, 2016; Monforti and Gonzalez-Aparicio, 2017). This work confirms the presence of the bias in MERRA2 and shows that the same bias is present in the ERA5 and JRA-3Q global reanalyses. Moreover, the bias is present in mesoscale datasets which perform dynamic downscaling. However, the magnitude of the bias is lower in mesoscale models.

We acknowledge that the use of 10 m winds and only two height levels in ERA5 and MERRA2 reanalyses might have introduced additional biases, especially for the highest observation campaigns reaching 200 m AGL. However, most of the campaigns used in this work reported winds at heights between 50 m and 125 m, which are closer to the upper height levels

of the models and therefore are less likely to be significantly affected by errors in vertical extrapolation. The identified wind biases in ERA5 and MERRA2 are similar to those in the other five model datasets. Moreover, these results are supported by the WRF modelling. Therefore, it is unlikely that biases in ERA5 and MERRA2 reanalyses related to the terrain elevation differences were artificially introduced by the use of 10 m winds and only two model levels.

More negative wind speed bias on hilltops and more positive wind speed bias in valleys has been observed before e.g. Jiménez and Dudhia (2012); Winstral et al. (2016). Previous studies (Schmidli et al., 2018; Carvalho et al., 2012; Saadatabadi et al., 2024) have suggested that the model performance in modelling winds is generally better if the model elevation matches the real-world elevation more closely. In this work, we establish the link between these two results. Namely, the wind speed bias is correlated with the elevation difference and modelled wind speeds can be adjusted in a controlled way by changing the model terrain elevation. Due to terrain smoothing in models, the absolute elevation of the valleys is higher and the absolute elevation of the hilltops is lower than the real-world elevation. It explains the differences of wind speed biases in valleys and on hilltops by the elevation difference between models and the real-world.

In the observation dataset used, measurements in Scandinavian Mountains and Southern Europe are generally performed in a locally more complex terrain with a higher $SD(z)$. Therefore, their elevation is likely to strongly differ from the elevation of the model grid-cell. Meanwhile, in Central European Plain observations are performed in more simpler terrain where $SD(z)$ is lower. Therefore, observations in Central European Plain are generally performed closer to the elevation of the model grid-cell. The distribution of the elevation differences is skewed towards locations where the real-world elevation is higher than the model elevation. Therefore, in simpler terrain observations campaigns are more likely to be located slightly above the model elevation, while in complex terrain observation campaigns are more likely to be located significantly higher above the model elevation. This can explain generally more negative wind speed bias in Scandinavian Mountains and Southern Europe and generally more positive bias in Central European Plain.

The results of this work show that wind speed and direction biases in models are correlated with the elevation difference between the model and the real-world. When two WRF models that used different terrain input data were compared, we observed a similar response of the modelled winds to the smoothing of the terrain as was present when the models were compared with the observations. It suggests that wind biases can potentially be fixed if the elevation in the model is modified to better match the real-world elevation. However, implications of modifying the model elevation on the overall model performance require further research. On the one hand, modifying the model elevation can improve the representation of other terrain features beyond the local elevation differences. These features include terrain slopes, terrain variability that affects resolved orographic drag, and large mountains that affect winds hundreds of kilometres downstream. The results of Schmidli et al. (2018) suggest that decreasing the smoothing intensity of the terrain can improve the model performance in modelling winds in complex terrain. On the other hand, smoothing of the terrain in atmospheric models is performed to avoid sharp terrain gradients, which can cause non-physical pressure gradients (Mahrer, 1984) or numerical instabilities (Bouëdec et al., 2025). Moreover, smoothing can potentially help average out uncertainties in the DEMs themselves. Therefore, the smoothing intensity of the terrain has to be balanced to keep the main features of the terrain well represented, while avoiding numerical artefacts.

The results of this work do not directly provide any information on the exact underlying physical processes that cause biases. It is likely that multiple physical processes are affected by differences in the representation of the terrain between models and the real-world. These processes are discussed in further paragraphs.

Since the terrain in the models is smoothed out, heights of the hills and depths of the valleys are generally underestimated in the models. If the height of the hill is underestimated in the model, the model underestimates orographic speed-up, which causes it to underestimate wind speeds. Errors in estimating orographic speed-up have been described as a potential cause of wind speed bias before (Jiménez and Dudhia, 2012).

Wind speed generally increases with height, and wind direction becomes more clockwise (in the Northern Hemisphere). If the height of the hill is underestimated in model, it is exposed to slower winds and more anti-clockwise wind direction. The relationship between topographic exposure and model wind speed biases has previously been observed by Pauscher et al. (2025). Topographic exposure is defined as the angle between the horizontal and the horizon when looking in a particular direction. It describes how exposed to or sheltered from winds the location is. A positive exposure angle indicates that the location is sheltered by the terrain, while a negative exposure angle indicates that it is exposed to winds.

Differences in topographic exposure can explain why the wind speed and direction biases are lower during the day than during the night. Assume that above the planetary boundary layer (PBL) wind flow is purely geostrophic with some wind speed and direction. Due to the friction force, near-surface winds are slower and more anti-clockwise (in the Northern Hemisphere). Within the PBL both wind speed and direction change continuously between these two values. If the atmosphere is more stable, less vertical mixing occurs, and the wind speed and direction change more uniformly throughout the boundary layer. On the other hand, if the atmosphere is unstable and the mixing is strong, strong vertical wind gradients occur near the very surface, and the change is slower at higher levels. Assume that an observation mast that measures wind speed at 100 m height above the ground level is located on top of a hill, that is 50 m above the model grid cell level. In the model the mast is exposed to winds at 100 m height, while in the real-world it is exposed to winds at 150 m height. During stable atmospheric conditions, the wind speed and direction differences between 100 m and 150 m heights are greater than during unstable conditions. Therefore, the difference between model output and observations is likely to be higher during stable conditions. Differences in topographic exposure can also explain the relationship between wind speed and wind direction biases.

The results of the analysis show that elevation differences have a stronger effect on both wind speed and wind direction biases in winter than in summer. In Europe in winter, the winds are generally stronger than in summer. Differences in topographic exposure and orographic speed-up have a stronger absolute effect on stronger winds, which can potentially explain differences in wind speed biases between summer and winter. Regarding the wind direction, a more positive wind speed bias can cause a stronger turbulent mixing, leading to a more clockwise wind direction bias.

Another possible cause of wind biases related to the terrain representation is differences between terrain slopes in the model and the real-world. Spatial aggregation of the terrain generally smooths out the slopes, which can affect multiple different processes. Duine et al. (2024) has shown that smoothing of the terrain in models significantly affects the modelled convective boundary layer heights. Moreover, smoothing of the slopes affects the dynamics of the slope related flows. Differences in terrain slopes affect solar radiation received by the surface, which affects vertical momentum transfer due to convection. If we assume

that the winds at higher levels of the atmosphere are modelled correctly, in the Northern Hemisphere models overestimating (underestimating) vertical transport of momentum can cause clockwise (anticlockwise) near-surface wind direction bias and positive (negative) wind speed bias (Sandu et al., 2020).

Our analysis shows that the elevation difference between models and the real-world statistically explains wind biases locally, i.e. within the same grid-cell. However, differences in terrain elevation can potentially influence modelled winds further downstream, which was not considered in our analysis.

Jiménez and Dudhia (2012) has previously noted that the WRF model overestimates wind speeds in valleys and underestimates wind speeds on top of hills. The study suggested and implemented wind correction using the Laplace of the elevation. Laplace of the elevation on a regular orthogonal grid is defined as:

$$\Delta h_{i,j} = \frac{h_{i-1,j} + h_{i+1,j} + h_{i,j-1} + h_{i,j+1} - 4 \cdot h_{i,j}}{dx^2}, \tag{7}$$

where dx is the horizontal grid spacing and $h_{i,j}$ is the elevation at the position indexed i, j. Positive Laplace indicates that the elevation of a grid-point is lower than the average of its neighbours, while negative Laplace indicates the elevation of a grid-point is higher than the average of its neighbours. The Laplace of the elevation was considered as the explanatory variable for model biases during the exploratory data analysis of this work. However, Laplace of the elevation showed weaker explanatory power than the elevation difference. When comparing principal components of the model difference, weighted differences in the Laplace of elevation showed correlations of 0.43 and 0.43 for values of PC1 of wind speed and wind direction, respectively. Compared to 0.69 and 0.56 for the case when weighted elevation difference is considered.

Jiménez and Dudhia (2012, 2013) have noted that the model performance in modelling winds in complex terrain can be significantly improved by choosing a more representative model grid point both horizontally and vertically. These studies have used a subjective approach, which cannot be generalised when assessing wind resources in larger areas. Choosing the appropriate model grid-point for representing the observation location should be physically justified. The results of this work suggest that choosing a nearby model grid-point that better matches the observation elevation has the potential to improve the wind speed bias. However, it cannot be guaranteed that there exists a model grid-point that matches the observation elevation. These studies also suggested choosing the appropriate grid-point not only horizontally, but also vertically. However, for wind energy applications, knowledge of the entire wind profile within the lowest few hundred metres is necessary, which would make the procedure of choice more complicated.

Microscale modelling has the potential to improve modelled winds in complex terrain. Due to higher resolution, microscale models can significantly reduce the elevation discrepancy. However, a significant limiting factor for microscale simulations is the computational costs. Mesoscale simulations can provide multiple decades of wind time-series over large geographical regions. However, computational fluid dynamics (CFD) simulations at microscale resolution are not feasible at such extents. Commonly, two microscale CFD modelling frameworks are used for wind resource modelling: Reynolds-averaged Navier-Stokes (RANS) and large eddy simulations (LES). While the RANS approach is computationally faster (Wagenbrenner et al., 2019), it struggles to model unsteady flows or cases where flow separation occurs (Sumner et al., 2010). Moreover, the results of the RANS simulations differ depending on the turbulence model used (Zou et al., 2022). On the other hand, LES provides more

accurate and consistent results, while being significantly more computationally expensive, especially during stable conditions (Bechmann and Sørensen, 2010).

Typically, an approach conceptually similar to measure-correlate-predict (MCP) (Woods and Watson, 1997) is used to produce long-term time-series from microscale CFD simulations. Only a few cases of characteristic wind conditions are fully simulated using the CFD approaches (Milla-Val et al., 2024). Later, simple statistics (Goyal and Ojha, 2011) or machine learning (Dujardin and Lehning, 2022) can be applied to the reference series such as mesoscale model output to construct the complete time-series that consider microscale effects. The accuracy of such an approach significantly depends on the accuracy of mesoscale model output (Travaglini et al., 2024), which is used both as the inlet conditions for modelling reference cases and as the reference time-series.

Microscale CFD approaches for wind resource assessment can be reasonably applied only to small geographical regions with a size on the order of kilometres. For wind resource assessment on a larger scale, the WAsP linear model can be applied, e.g. (Dörenkämper et al., 2020). However, the study has reported that the linear model largely overestimates winds in the most complex orography, since the assumptions of the linear model do not hold. Moreover, the approach works only with temporally averaged winds depending on the wind direction, which does not directly produce the complete time-series.

An important aspect to consider when downscaling mesoscale wind data to microscale, is how to harmonize the elevation description between the two approaches. Before applying the WAsP linear model, the wind climate is generalised, i.e. microscale terrain effects that are resolved by the mesoscale model are removed (Floors et al., 2025). Similarly, when applying CFD downscaling, terrain differences between the mesoscale and microscale models have to be considered. Our results suggest that terrain discrepancies affect both wind speed and direction, and the strength of the effect depends on the time of day and the month of the year.

5 Conclusions

In this work, a large dataset of tall-mast and remote sensing device wind observations was used to address systematic issues of multiple atmospheric model datasets. To the authors' knowledge, such large scale comparisons between modelled and observed winds at wind turbine rotor heights have not been conducted before. It was shown that all seven different atmospheric models share the same bias when modelling wind speeds at wind turbine rotor heights. Models generally underestimate wind speeds in mountainous regions — Scandinavian mountains and Southern Europe, while overestimating them in the Central European Plain. Moreover, it was shown that the diurnal and seasonal cycles of wind speed biases also differ between these parts of Europe. It was observed that wind direction biases share the same diurnal and spatial patterns as wind speed biases.

The elevation difference between the models and the real-world terrain can explain a significant part of the model biases. The PC1 of wind speed biases explains between 61.1% and 82.5% of variance in model biases between observation locations depending on the model dataset. The values of PC1 of wind speed biases shows a correlation with the elevation difference between 0.27 and 0.71 depending on the model dataset. Comparison between two different models allowed to estimate that the elevation difference of 100 m has an effect between 0.1 and 0.9 $\mathrm{m\,s^{-1}}$ on the wind speed bias and an effect between 0.4° and

5.6° on the wind direction bias. The magnitude of the effect depends on the time of day and month of year. The magnitude of the effect of the elevation difference on bias when comparing models and observations is similar in magnitude to the case when two models are compared. It should be noted that we considered only the average magnitude of the diurnal bias in the region. However, the intensity of the diurnal cycle of the bias at a particular location can also depend on the land-cover type, which we did not consider in our analysis.

The spatial differences of biases between the Central European Plain and mountainous regions (Scandinavian Mountains and Southern Europe) can be explained by the fact that the dataset is biassed towards observation campaigns that are located at locally higher elevations, where real-world elevation exceeds the model elevation. In mountainous regions, the magnitude of the differences between real-world and model terrain elevation is higher, leading to stronger biases. These differences in height influence how several physical processes are represented in the model, which impact modelled winds.

We used the elevation difference between the model and the real-world terrain as a measure of how terrain differs between models and the real-world. It directly describes the effects of the elevation differences on changes in topographic exposure and orographic speed-up due to terrain smoothing. Moreover, it indirectly contains information about how strong slopes are affected locally, influencing modelled slope flows and resolved orographic drag. However, it cannot fully describe the complicated nature of flow changes in complex terrain due to smoothing of the terrain. The results of this work cannot distinguish the contribution of different physical processes to this wind bias. However, the results suggest that the bias can possibly be improved by modifying the model terrain so that it matches the real-world terrain elevation more closely. More research is needed to identify the effects of terrain smoothing on modelled winds, since smoothing of the terrain in mesoscale models is done to reduce numerical artefacts.

Data availability. Observation data from the EMD internal mast database and EMD-EUR+ dataset are not publicly available. Data from NORA3 model dataset is available from https://thredds.met.no/thredds/projects/nora3.html. Data from CERRA reanalysis is available from https://cds.climate.copernicus.eu/datasets/reanalysis-cerra-height-levels. Data from ERA5 reanalysis is available from https://cds.climate.copernicus.eu/datasets/reanalysis-era5-single-levels. Data from MERRA2 reanalysis is available from https://disc.gsfc.nasa.gov/datasets?project=MERRA-2. Data from NEWA model dataset is available from https://map.neweuropeanwindatlas.eu/. Data from JRA-3Q reanalysis is available from https://gdex.ucar.edu/datasets/d640001/.

Appendix A: WRF setup

Table A1. Setup of the WRF models used in this work.

WRF version	4.5.1.
Domain	Single 810×1620 km domain centred on Sweden.
Grid	3 km grid spacing. 270×540 grid cells. 10 cell wide buffer zone at the boundary.
Vertical levels	50
Simulation length	Simulation covering the entire 2011 stitching together 48 h runs with 6 h spin-up.
Terrain data	GMTED2010 with 30″ and 5′ resolution
Dynamical forcing	Hourly ERA5 data on surface and pressure levels
Time step	12 s
PBL scheme	MYJ
Surface layer scheme	Eta Similarity
Land surface model	Noah
Cloud microphysics scheme	Ferrier Eta
Radiation scheme	RRTMG
Cumulus scheme	None

Appendix B: Results of PCA for all model datasets

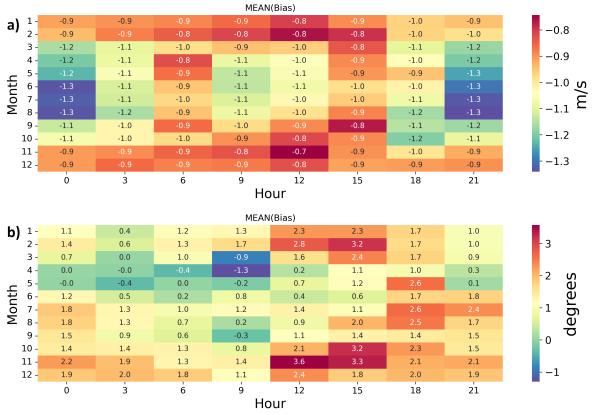

Figure B1. Spatially averaged wind speed biases (in $\mathrm{m\,s^{-1}}$) (a) and wind direction biases (in degrees) (b) in JRA-3Q reanalysis dependent on month (y axis) and time of day (x axis).

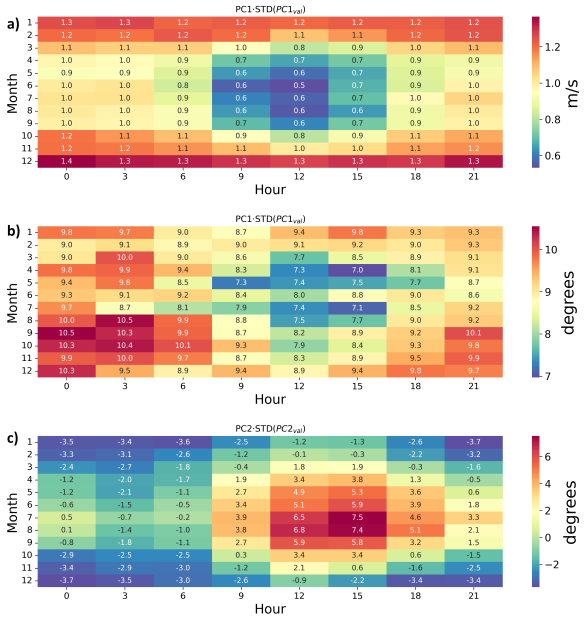

Figure B2. JRA-3Q reanalysis and observation comparison. Loadings of the PC1 for wind speed bias (a), PC1 of wind direction bias (b) and PC2 of wind direction bias (c). Multiplied by the standard deviation of values of the corresponding PC.

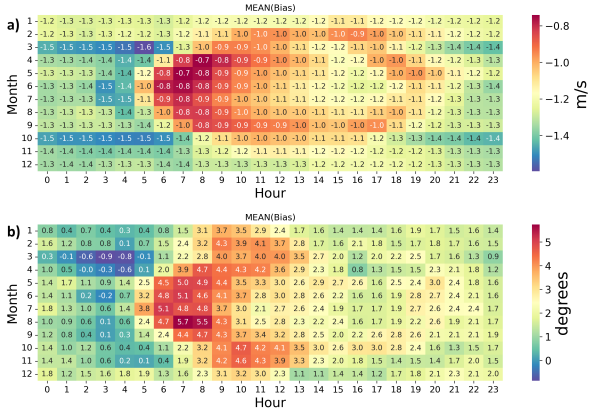

Figure B3. Spatially averaged wind speed biases (in $\mathrm{m\,s^{-1}}$) (a) and wind direction biases (in degrees) (b) in MERRA2 reanalysis dependent on month (y axis) and time of day (x axis).

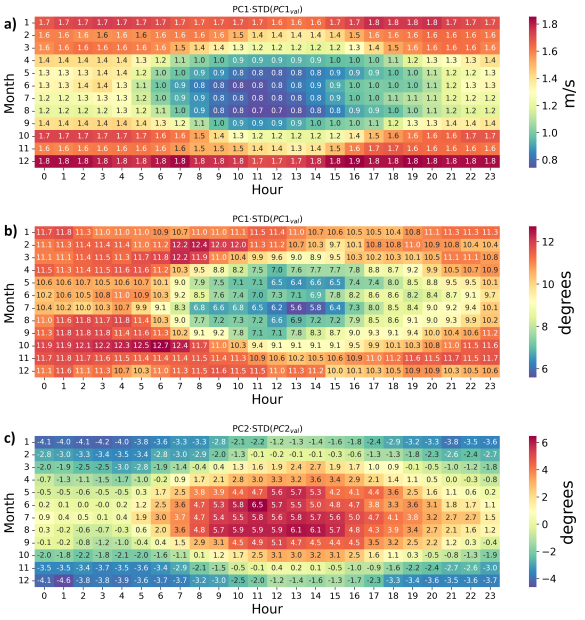

Figure B4. MERRA2 reanalysis and observation comparison. Loadings of the PC1 for wind speed bias (a), PC1 of wind direction bias (b) and PC2 of wind direction bias (c). Multiplied by the standard deviation of values of the corresponding PC.

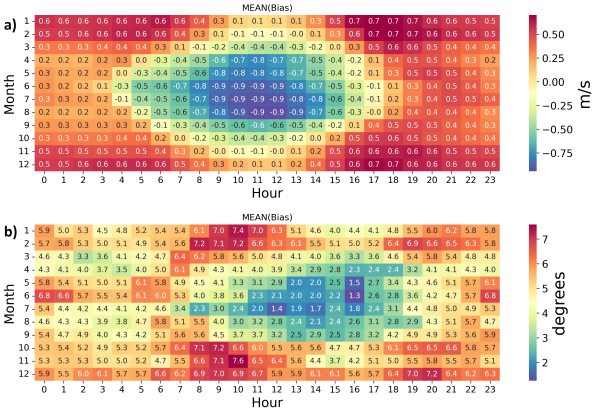

Figure B5. Spatially averaged wind speed biases (in $\mathrm{m\,s^{-1}}$) (a) and wind direction biases (in degrees) (b) in NEWA model dataset dependent on month (y axis) and time of day (x axis).

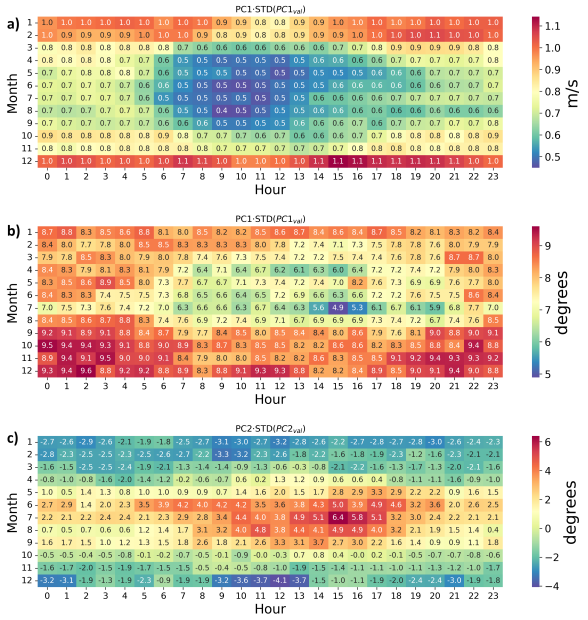

Figure B6. NEWA model dataset and observation comparison. Loadings of the PC1 for wind speed bias (a), PC1 of wind direction bias (b) and PC2 of wind direction bias (c). Multiplied by the standard deviation of values of the corresponding PC.

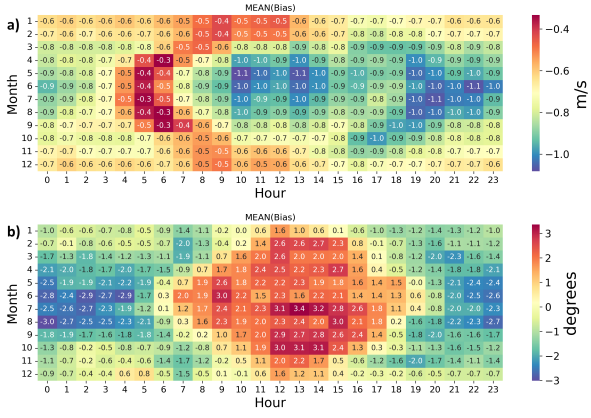

Figure B7. Spatially averaged wind speed biases (in m s^{-1}) (a) and wind direction biases (in degrees) (b) in CERRA model dataset dependent on month (y axis) and time of day (x axis).

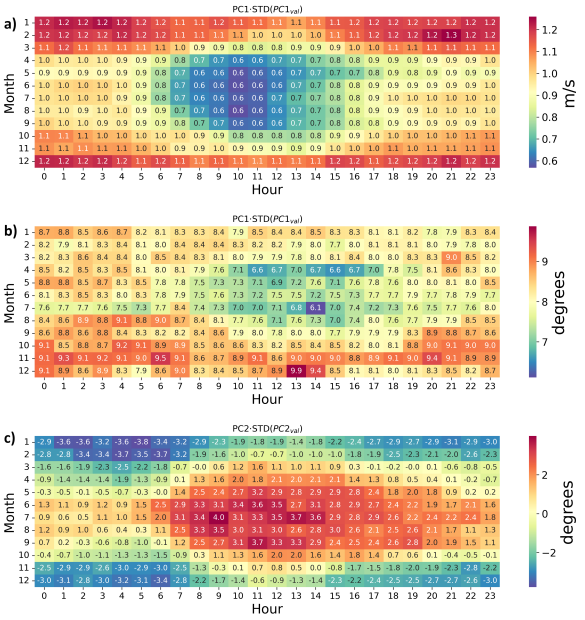

Figure B8. CERRA model dataset and observation comparison. Loadings of the PC1 for wind speed bias (a), PC1 of wind direction bias (b) and PC2 of wind direction bias (c). Multiplied by the standard deviation of values of the corresponding PC.

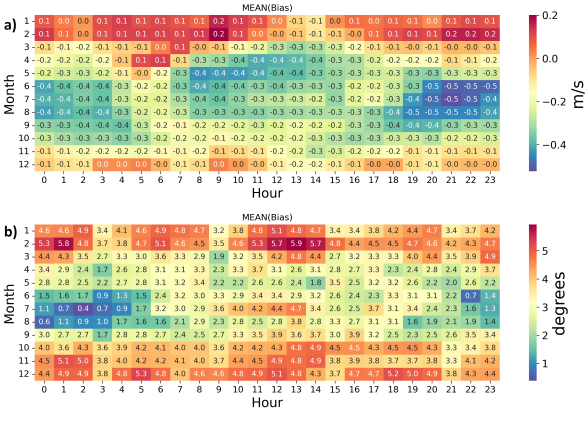

Figure B9. Spatially averaged wind speed biases (in m s^{-1}) (a) and wind direction biases (in degrees) (b) in NORA3 model dataset dependent on month (y axis) and time of day (x axis).

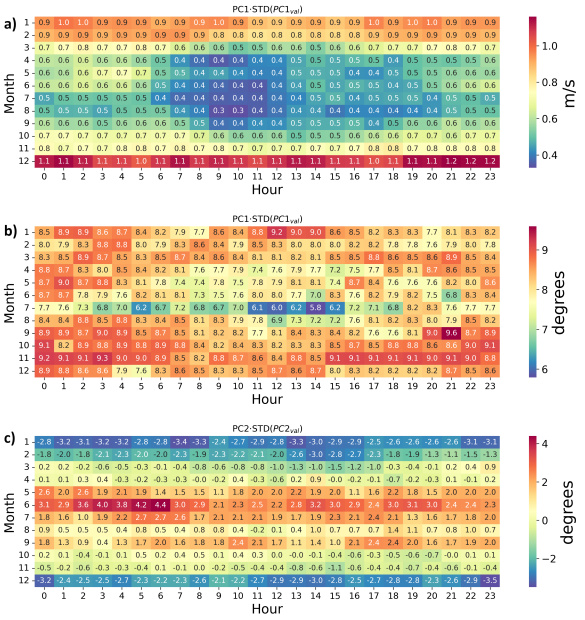

Figure B10. NORA3 model dataset and observation comparison. Loadings of the PC1 for wind speed bias (a), PC1 of wind direction bias (b) and PC2 of wind direction bias (c). Multiplied by the standard deviation of values of the corresponding PC.

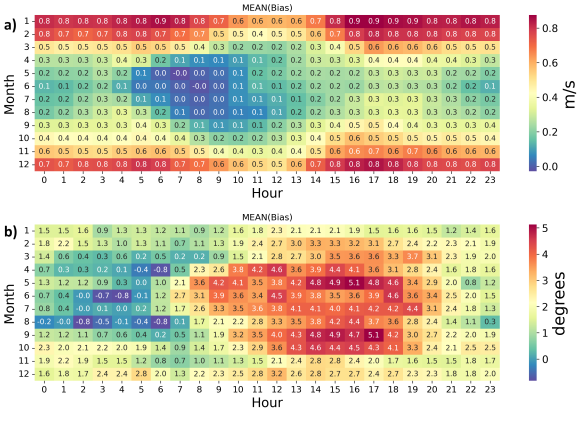

Figure B11. Spatially averaged wind speed biases (in $\mathrm{m\,s^{-1}}$) (a) and wind direction biases (in degrees) (b) in EMD-EUR+ model dataset dependent on month (y axis) and time of day (x axis).

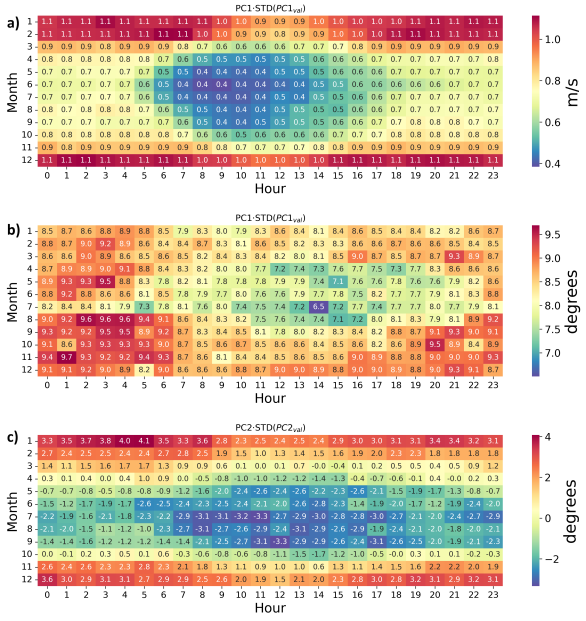

Figure B12. EMD-EUR+ model dataset and observation comparison. Loadings of the PC1 for wind speed bias (a), PC1 of wind direction bias (b) and PC2 of wind direction bias (c). Multiplied by the standard deviation of values of the corresponding PC.

Author contributions. MP designed the study, performed model comparison against measurements, performed WRF simulations, analysed the results, prepared the figures. TS, LS and AH provided scientific supervision. MP wrote the draft for the manuscript. All authors contributed to the final version of the manuscript.

Competing interests. MP and LS work at the EMD International A/S, which commercially provides data from the EMD-EUR+ model dataset and EMD's internal mast database. AH is a member of the editorial board of Wind Energy Science.

Acknowledgements. Maksims Pogumirskis has received funding from the European Union's Horizon Europe research and innovation programme (HORIZON-MSCA-2022-DN-01-01) under the Marie Sklodowska-Curie grant agreement no. 101119550 (AptWind).

References

Terrain Effects on Wind Flow: Simulations With an Immersed Boundary Method, vol. Volume 1: Aircraft Engine; Ceramics; Coal, Biomass and Alternative Fuels; Wind Turbine Technology of *Turbo Expo*, https://doi.org/10.1115/GT2011-46240, 2011.

Backwell, B., Clarke, E., Ladwa, R., Mullin, S., Jayasurya, F., and Hutchinson, M.: Global Wind Report 2025, Tech. rep., Global Wind Energy Council, Lisbon, Portugal, 2025.

Bechmann, A. and Sørensen, N. N.: Hybrid RANS/LES method for wind flow over complex terrain, Wind Energy, 13, 36–50, https://doi.org/https://doi.org/10.1002/we.346, 2010.

Belmonte Rivas, M. and Stoffelen, A.: Characterizing ERA-Interim and ERA5 surface wind biases using ASCAT, Ocean Science, 15, 831–852, https://doi.org/10.5194/os-15-831-2019, 2019.

Bethere, L., Sennikovs, J., and Bethers, U.: Climate indices for the Baltic states from principal component analysis, Earth System Dynamics, 8, 951–962, https://doi.org/10.5194/esd-8-951-2017, 2017.

Bouëdec, E. L., Chemel, C., and Staquet, C.: Dealing with steep slopes when modeling stable boundary-layer flow in Alpine terrain, Quarterly Journal of the Royal Meteorological Society, 151, e4835, https://doi.org/https://doi.org/10.1002/qj.4835, 2025.

Carvalho, D.: An Assessment of NASA's GMAO MERRA-2 Reanalysis Surface Winds, Journal of Climate, 32, 8261–8281, https://doi.org/10.1175/JCLI-D-19-0199.1, 2019.

Carvalho, D., Rocha, A., Gómez-Gesteira, M., and Santos, C.: A sensitivity study of the WRF model in wind simulation for an area of high wind energy, Environmental Modelling & Software, 33, 23–34, https://doi.org/https://doi.org/10.1016/j.envsoft.2012.01.019, 2012.

Cheynet, E., Solbrekke, I. M., Diezel, J. M., and Reuder, J.: A one-year comparison of new wind atlases over the North Sea, Journal of Physics: Conference Series, 2362, 012 009, https://doi.org/10.1088/1742-6596/2362/1/012009, 2022.

Cheynet, E., Diezel, J. M., Haakenstad, H., Breivik, Ø., Peña, A., and Reuder, J.: Tall wind profile validation of ERA5, NORA3, and NEWA datasets using lidar observations, Wind Energy Science, 10, 733–754, https://doi.org/10.5194/wes-10-733-2025, 2025.

Danielson, J. J. and Gesch, D. B.: Global Multi-resolution Terrain Elevation Data 2010 (GMTED2010), Open-File Report 2011–1073, U.S. Geological Survey, https://doi.org/10.3133/ofr20111073, 2011.

Das, A. and Baidya Roy, S.: JRA55 is the best reanalysis representing observed near-surface wind speeds over India, Atmospheric Research, 297, 107 111, https://doi.org/https://doi.org/10.1016/j.atmosres.2023.107111, 2024.

Dörenkämper, M., Olsen, B. T., Witha, B., Hahmann, A. N., Davis, N. N., Barcons, J., Ezber, Y., García-Bustamante, E., González-Rouco, J. F., Navarro, J., Sastre-Marugán, M., Sīle, T., Trei, W., Žagar, M., Badger, J., Gottschall, J., Sanz Rodrigo, J., and Mann, J.: The Making of the New European Wind Atlas – Part 2: Production and evaluation, Geoscientific Model Development, 13, 5079–5102, https://doi.org/10.5194/gmd-13-5079-2020, 2020.

Draxl, C., Worsnop, R. P., Xia, G., Pichugina, Y., Chand, D., Lundquist, J. K., Sharp, J., Wedam, G., Wilczak, J. M., and Berg, L. K.: Mountain waves can impact wind power generation, Wind Energy Science, 6, 45–60, https://doi.org/10.5194/wes-6-45-2021, 2021.

Duine, G.-J., De Wekker, S. F. J., and Knievel, J. C.: The Influence of Terrain Smoothing on Simulated Convective Boundary-Layer Depths in Mountainous Terrain, Atmosphere, 15, https://doi.org/10.3390/atmos15020145, 2024.

Dujardin, J. and Lehning, M.: Wind-Topo: Downscaling near-surface wind fields to high-resolution topography in highly complex terrain with deep learning, Quarterly Journal of the Royal Meteorological Society, 148, 1368–1388, https://doi.org/https://doi.org/10.1002/qj.4265, 2022.

ECMWF: IFS Documentation CY41R2 - Part IV: Physical Processes, 4, European Centre for Medium-Range Weather Forecasts, https://doi.org/10.21957/tr5rv27xu, 2016.

European Commission: Commission sets out immediate actions to support the European wind power industry, https://ec.europa.eu/commission/presscorner/detail/en/ip_23_5185, accessed: 2025-03-24, 2023.

Fahrland, E.: Copernicus DEM, Copernicus Digital Elevation Model, Product Handbook, Tech. rep., AIRBUS, https://dataspace.copernicus.eu/sites/default/files/media/files/2024-06/geo1988-copernicusdem-spe-002_producthandbook_i5.0.pdf, 2022.

Fernández-González, S., Martín, M. L., García-Ortega, E., Merino, A., Lorenzana, J., Sánchez, J. L., Valero, F., and Rodrigo, J. S.: Sensitivity Analysis of the WRF Model: Wind-Resource Assessment for Complex Terrain, Journal of Applied Meteorology and Climatology, 57, 733 – 753, https://doi.org/10.1175/JAMC-D-17-0121.1, 2018.

Floors, R. R., Davis, N., Olsen, B. T., Badger, J., and Hansen, B. O.: Global Wind Atlas v4: Generalized Wind Climates, https://doi.org/10.11583/DTU.28945943.v1, 2025.

Gelaro, R., McCarty, W., Suárez, M. J., Todling, R., Molod, A., Takacs, L., Randles, C. A., Darmenov, A., Bosilovich, M. G., Reichle, R., Wargan, K., Coy, L., Cullather, R., Draper, C., Akella, S., Buchard, V., Conaty, A., da Silva, A. M., Gu, W., Kim, G.-K., Koster, R., Lucchesi, R., Merkova, D., Nielsen, J. E., Partyka, G., Pawson, S., Putman, W., Rienecker, M., Schubert, S. D., Sienkiewicz, M., and Zhao, B.: "The Modern-Era Retrospective Analysis for Research and Applications, Version 2 (MERRA-2)", Journal of Climate, 30, 5419 – 5454, https://doi.org/10.1175/JCLI-D-16-0758.1, 2017.

Gómez-Navarro, J. J., Raible, C. C., and Dierer, S.: Sensitivity of the WRF model to PBL parametrisations and nesting techniques: evaluation of wind storms over complex terrain, Geoscientific Model Development, 8, 3349–3363, https://doi.org/10.5194/gmd-8-3349-2015, 2015.

Goyal, M. K. and Ojha, C. S. P.: Evaluation of linear regression methods as downscaling tools in temperature projections over the Pichola Lake Basin in India, Hydrological Processes, 25, 1453–1465, https://doi.org/https://doi.org/10.1002/hyp.7911, 2011.

Gualtieri, G.: Reliability of ERA5 Reanalysis Data for Wind Resource Assessment: A Comparison against Tall Towers, Energies, 14, https://doi.org/10.3390/en14144169, 2021.

Haakenstad, H., Øyvind Breivik, Furevik, B. R., Reistad, M., Bohlinger, P., and Aarnes, O. J.: NORA3: A Nonhydrostatic High-Resolution Hindcast of the North Sea, the Norwegian Sea, and the Barents Sea, Journal of Applied Meteorology and Climatology, 60, 1443 – 1464, https://doi.org/10.1175/JAMC-D-21-0029.1, 2021.

Hahmann, A. N., Sīle, T., Witha, B., Davis, N. N., Dörenkämper, M., Ezber, Y., García-Bustamante, E., González-Rouco, J. F., Navarro, J., Olsen, B. T., and Söderberg, S.: The making of the New European Wind Atlas – Part 1: Model sensitivity, Geoscientific Model Development, 13, 5053–5078, https://doi.org/10.5194/gmd-13-5053-2020, 2020.

Hersbach, H., Bell, B., Berrisford, P., Hirahara, S., Horányi, A., Muñoz-Sabater, J., Nicolas, J., Peubey, C., Radu, R., Schepers, D., Simmons, A., Soci, C., Abdalla, S., Abellan, X., Balsamo, G., Bechtold, P., Biavati, G., Bidlot, J., Bonavita, M., De Chiara, G., Dahlgren, P., Dee, D., Diamantakis, M., Dragani, R., Flemming, J., Forbes, R., Fuentes, M., Geer, A., Haimberger, L., Healy, S., Hogan, R. J., Hólm, E., Janisková, M., Keeley, S., Laloyaux, P., Lopez, P., Lupu, C., Radnoti, G., de Rosnay, P., Rozum, I., Vamborg, F., Villaume, S., and Thépaut, J.-N.: The ERA5 global reanalysis, Quarterly Journal of the Royal Meteorological Society, 146, 1999–2049, https://doi.org/https://doi.org/10.1002/qj.3803, 2020.

Hollingsworth, A.: Validation and diagnosis of atmospheric models, Dynamics of Atmospheres and Oceans, 20, 227–246, https://doi.org/https://doi.org/10.1016/0377-0265(94)90019-1, forecasting weather and climate since, 1994.

Hu, W., Scholz, Y., Yeligeti, M., Bremen, L., and Deng, Y.: Downscaling ERA5 wind speed data: a machine learning approach considering topographic influences, Environmental Research Letters, 18, https://doi.org/10.1088/1748-9326/aceb0a, 2023.

Jiménez, P. A. and Dudhia, J.: Improving the Representation of Resolved and Unresolved Topographic Effects on Surface Wind in the WRF Model, Journal of Applied Meteorology and Climatology, 51, 300 – 316, https://doi.org/10.1175/JAMC-D-11-084.1, 2012.

Jiménez, P. A. and Dudhia, J.: On the Ability of the WRF Model to Reproduce the Surface Wind Direction over Complex Terrain, Journal of Applied Meteorology and Climatology, 52, 1610 – 1617, https://doi.org/10.1175/JAMC-D-12-0266.1, 2013.

Jolliffe, I. T.: Principal Component Analysis, Springer Series in Statistics, Springer New York, NY, 2 edn., ISBN 978-0-387-95442-4, https://doi.org/10.1007/b98835, springer Science+Business Media, Published: 01 October 2002, 2002.

Jourdier, B.: Evaluation of ERA5, MERRA-2, COSMO-REA6, NEWA and AROME to simulate wind power production over France, Advances in Science and Research, 17, 63–77, https://doi.org/10.5194/asr-17-63-2020, 2020.

Jourdier, B., Diaz, C., and Dubus, L.: Evaluation of CERRA for wind energy applications, in: EMS Annual Meeting 2023, Bratislava, Slovakia, https://doi.org/10.5194/ems2023-311, 2023.

Kalverla, P. C., Holtslag, A. A. M., Ronda, R. J., and Steeneveld, G.-J.: Quality of wind characteristics in recent wind atlases over the North Sea, Quarterly Journal of the Royal Meteorological Society, 146, 1498–1515, https://doi.org/https://doi.org/10.1002/qj.3748, 2020.

Klaver, R., Haarsma, R., Vidale, P. L., and Hazeleger, W.: Effective resolution in high resolution global atmospheric models for climate studies, Atmospheric Science Letters, 21, e952, https://doi.org/https://doi.org/10.1002/asl.952, 2020.

Knoop, S., Bosveld, F. C., de Haij, M. J., and Apituley, A.: A 2-year intercomparison of continuous-wave focusing wind lidar and tall mast wind measurements at Cabauw, Atmospheric Measurement Techniques, 14, 2219–2235, https://doi.org/10.5194/amt-14-2219-2021, 2021.

Kosaka, Y., Kobayashi, S., Harada, Y., Kobayashi, C., Naoe, H., Yoshimoto, K., Harada, M., Goto, N., Chiba, J., Miyaoka, K., Sekiguchi, R., Deushi, M., Kamahori, H., Nakaegawa, T., Tanaka, T. Y., Tokuhiro, T., Sato, Y., Matsushita, Y., and Onogi, K.: The JRA-3Q Reanalysis, Journal of the Meteorological Society of Japan. Ser. II, 102, 49–109, https://doi.org/10.2151/jmsj.2024-004, 2024.

Kuru, S.: Evaluating the accuracy of NEWA, ERA5 and NORA3 in predicting onshore wind conditions: a comparative study using ICOS meteorological mast data in Sweden, Master of science dissertation, Uppsala University, Department of Earth Sciences, Campus Gotland, Uppsala, Sweden, 2023.

Laurila, T. K., Sinclair, V. A., and Gregow, H.: Climatology, variability, and trends in near-surface wind speeds over the North Atlantic and Europe during 1979–2018 based on ERA5, International Journal of Climatology, 41, 2253–2278, https://doi.org/https://doi.org/10.1002/joc.6957, 2021.

Le Toumelin, L., Gouttevin, I., Galiez, C., and Helbig, N.: A two-fold deep-learning strategy to correct and downscale winds over mountains, Nonlinear Processes in Geophysics, 31, 75–97, https://doi.org/10.5194/npg-31-75-2024, 2024.

Mahrer, Y.: An Improved Numerical Approximation of the Horizontal Gradients in a Terrain-Following Coordinate System, Monthly Weather Review, 112, 918 – 922, https://doi.org/10.1175/1520-0493(1984)112<0918:AINAOT>2.0.CO;2, 1984.

Meadows, M., Jones, S., and Reinke, K.: Vertical accuracy assessment of freely available global DEMs (FABDEM, Copernicus DEM, NASADEM, AW3D30 and SRTM) in flood-prone environments, International Journal of Digital Earth, 17, 2308 734, https://doi.org/10.1080/17538947.2024.2308734, 2024.

MEASNET: Evaluation of Site-Specific Wind Conditions, Tech. rep., Campus de Montegancedo. EDIFICIO “CIDA”., Madrid, Spain, 2022.

Meyer, P. J. and Gottschall, J.: How do NEWA and ERA5 compare for assessing offshore wind resources and wind farm siting conditions?, Journal of Physics: Conference Series, 2151, 012 009, https://doi.org/10.1088/1742-6596/2151/1/012009, 2022.

Mi, X. and Liu, P.: A Comparative Study of Near-Surface Wind Speed Observations and Reanalysis Datasets in China Over the Past 38 Years, International Journal of Climatology, https://doi.org/https://doi.org/10.1002/joc.8738, 2024.

Miao, H., Dong, D., Huang, G., Hu, K., Tian, Q., and Gong, Y.: Evaluation of Northern Hemisphere surface wind speed and wind power density in multiple reanalysis datasets, Energy, 200, 117 382, https://doi.org/https://doi.org/10.1016/j.energy.2020.117382, 2020.

Milla-Val, J., Montañés, C., and Fueyo, N.: Economical microscale predictions of wind over complex terrain from mesoscale simulations using machine learning, Modeling Earth Systems and Environment, 10, 1407–1421, 2024.

Möhrlen, C., Zack, J., Browell, J., Wilbert, S., Wirth, I., and Felder, M.: Recommended Practice for the Implementation of Renewable Energy Forecasting Solutions, Tech. rep., IEA Wind, https://iea-wind.org/wp-content/uploads/2022/06/IEAWind_Task36_Recommended_Practice_Part4_1st_Edition_public.pdf, 2022.

Monforti, F. and Gonzalez-Aparicio, I.: Comparing the impact of uncertainties on technical and meteorological parameters in wind power time series modelling in the European Union, Applied Energy, 206, 439–450, https://doi.org/https://doi.org/10.1016/j.apenergy.2017.08.217, 2017.

Owens, R. G. and Hewson, T. D.: ECMWF Forecast User Guide, ECMWF, https://doi.org/10.21957/m1cs7h, 2018.

Pauscher, L., Geiger, D., Wirth, M., Yuan, D., Weber, H., and Callies, D.: Downscaling reanalysis models using a simple data-driven approach based on topography and atmospheric conditions, in: Proceedings of the Wind Energy Science Conference (WESC 2025), Wind Energy Science Conference, Nantes, France, 24–27 June 2025, 2025.

Pogumirskis, M., Sīle, T., Seņņikovs, J., and Bethers, U.: PCA analysis of wind direction climate in the baltic states, Tellus A: Dynamic Meteorology and Oceanography, 73, 1–16, https://doi.org/10.1080/16000870.2021.1962490, 2021.

Ramon, J., Lledó, L., Torralba, V., Soret, A., and Doblas-Reyes, F. J.: What global reanalysis best represents near-surface winds?, Quarterly Journal of the Royal Meteorological Society, 145, 3236–3251, https://doi.org/https://doi.org/10.1002/qj.3616, 2019.

Ramon, J., Lledó, L., Pérez-Zanón, N., Soret, A., and Doblas-Reyes, F. J.: The Tall Tower Dataset: a unique initiative to boost wind energy research, Earth System Science Data, 12, 429–439, https://doi.org/10.5194/essd-12-429-2020, 2020.

Ridal, M., Bazile, E., Le Moigne, P., Randriamampianina, R., Schimanke, S., Andrae, U., Berggren, L., Brousseau, P., Dahlgren, P., Edvinsson, L., El-Said, A., Glinton, M., Hagelin, S., Hopsch, S., Isaksson, L., Medeiros, P., Olsson, E., Unden, P., and Wang, Z. Q.: CERRA, the Copernicus European Regional Reanalysis system, Quarterly Journal of the Royal Meteorological Society, 150, 3385–3411, https://doi.org/https://doi.org/10.1002/qj.4764, 2024.

Rouholahnejad, F., Meyer, P. J., and Gottschall, J.: Collocating wind data: A case study on the verification of the CERRA dataset, Journal of Physics: Conference Series, 2875, 012 016, https://doi.org/10.1088/1742-6596/2875/1/012016, 2024.

Saadatabadi, A. R., Hamzeh, N. H., Kaskaoutis, D. G., Ghasabi, Z., Penchah, M. M., Sotiropoulou, R.-E. P., and Habibi, M.: Optimization and Evaluation of the Weather Research and Forecasting (WRF) Model for Wind Energy Resource Assessment and Mapping in Iran, Applied Sciences, 14, https://doi.org/10.3390/app14083304, 2024.

Sandu, I., Zadra, A., and Wedi, N.: Impact of orographic drag on forecast skill, ECMWF Newsletter, 150, published January 2017, 2017.

Sandu, I., Bechtold, P., Nuijens, L., Beljaars, A., and Brown, A.: On the causes of systematic forecast biases in near-surface wind direction over the oceans, https://doi.org/10.21957/wggbl43u, 2020.

Schmidli, J., Böing, S., and Fuhrer, O.: Accuracy of Simulated Diurnal Valley Winds in the Swiss Alps: Influence of Grid Resolution, Topography Filtering, and Land Surface Datasets, Atmosphere, 9, https://doi.org/10.3390/atmos9050196, 2018.

Shaw, J. and Weller, H.: Comparison of Terrain-Following and Cut-Cell Grids Using a Nonhydrostatic Model, Monthly Weather Review, 144, 2085 – 2099, https://doi.org/10.1175/MWR-D-15-0226.1, 2016.

Skamarock, W. C.: Evaluating Mesoscale NWP Models Using Kinetic Energy Spectra, Monthly Weather Review, 132, 3019 – 3032, https://doi.org/10.1175/MWR2830.1, 2004.

Solbakken, K., Birkelund, Y., and Samuelsen, E. M.: Evaluation of surface wind using WRF in complex terrain: Atmospheric input data and grid spacing, Environmental Modelling & Software, 145, 105 182, https://doi.org/https://doi.org/10.1016/j.envsoft.2021.105182, 2021.

Solbrekke, I. M., Sorteberg, A., and Haakenstad, H.: The 3 km Norwegian reanalysis (NORA3) – a validation of offshore wind resources in the North Sea and the Norwegian Sea, Wind Energy Science, 6, 1501–1519, https://doi.org/10.5194/wes-6-1501-2021, 2021.

Spangehl, T., Borsche, M., Niermann, D., Kaspar, F., Schimanke, S., Brienen, S., Möller, T., and Brast, M.: Intercomparing the quality of recent reanalyses for offshore wind farm planning in Germany's exclusive economic zone of the North Sea, Advances in Science and Research, 20, 109–128, https://doi.org/10.5194/asr-20-109-2023, 2023.

Staffell, I. and Pfenninger, S.: Using bias-corrected reanalysis to simulate current and future wind power output, Energy, 114, 1224–1239, https://doi.org/https://doi.org/10.1016/j.energy.2016.08.068, 2016.

Sumner, J., Watters, C. S., and Masson, C.: CFD in Wind Energy: The Virtual, Multiscale Wind Tunnel, Energies, 3, 989–1013, https://doi.org/10.3390/en3050989, 2010.

Svenningsen, L., Thøgersen, M., and Sørensen, T.: Validation of EMD-WRF EUROPE+ (ERA5) mesoscale dataset, Tech. rep., EMD International A/S, https://help.emd.dk/knowledgebase/content/TechNotes/TechnicalNote7_EMDWRF_EUROPE_Validation.pdf, 2020.

Torralba, V., Doblas-Reyes, F. J., and Gonzalez-Reviriego, N.: Uncertainty in recent near-surface wind speed trends: a global reanalysis intercomparison, Environmental Research Letters, 12, 114 019, https://doi.org/10.1088/1748-9326/aa8a58, 2017.

Travaglini, R., Melani, P. F., Balduzzi, F., Orlando, S., Viti, V., and Bianchini, A.: A critical insight into the most effective CFD settings to model atmospheric stability in wind energy applications, Journal of Physics: Conference Series, 2767, 092 031, https://doi.org/10.1088/1742-6596/2767/9/092031, 2024.

United Nations Climate Change (UNFCCC): The Paris Agreement, https://unfccc.int/process-and-meetings/the-paris-agreement, accessed: 2025-03-24.

Wagenbrenner, N. S., Forthofer, J. M., Page, W. G., and Butler, B. W.: Development and Evaluation of a Reynolds-Averaged Navier–Stokes Solver in WindNinja for Operational Wildland Fire Applications, Atmosphere, 10, https://doi.org/10.3390/atmos10110672, 2019.

Weigel, A. P., Liniger, M. A., and Appenzeller, C.: Can multi-model combination really enhance the prediction skill of probabilistic ensemble forecasts?, Quarterly Journal of the Royal Meteorological Society, 134, 241–260, https://doi.org/https://doi.org/10.1002/qj.210, 2008.

Williams, R., Zhao, F., Melkonyan, N., Hutchinson, M., and Cheong, J.: Global Offshore Wind Report 2025, Tech. rep., Global Wind Energy Council, Lisbon, Portugal, 2025.

Winstral, A., Jonas, T., and Helbig, N.: Statistical Downscaling of Gridded Wind Speed Data Using Local Topography, Journal of Hydrometeorology, 18, https://doi.org/10.1175/JHM-D-16-0054.1, 2016.

Woods, J. and Watson, S.: A new matrix method of predicting long-term wind roses with MCP, Journal of Wind Engineering and Industrial Aerodynamics, 66, 85–94, https://doi.org/https://doi.org/10.1016/S0167-6105(97)00009-3, 1997.

Yamaguchi, A., Tavana, A., and Ishihara, T.: Assessment of Wind over Complex Terrain Considering the Effects of Topography, Atmospheric Stability and Turbine Wakes, Atmosphere, 15, https://doi.org/10.3390/atmos15060723, 2024.

Zhi, M. H.: Accuracy of Energy Estimation for Small Wind Farms Based on Mesoscale Wind Data, Bachelor of science dissertation, Uppsala University, Department of Earth Sciences, Campus Gotland, 2023.

Zou, Y., Yue, P., Liu, Q., He, X., and Wang, Z.: Wind Field Characteristics of Complex Terrain Based on Experimental and Numerical Investigation, Applied Sciences, 12, https://doi.org/10.3390/app12105124, 2022.